5-2013

Production of high yield gold/gold-sulfide nanoparticles via cellulose membrane.

Kurtis T. James
University of Louisville

PRODUCTION OF HIGH YIELD GOLD/GOLD-SULFIDE NANOPARTICLES VIA CELLULOSE MEMBRANE

By

Kurtis T. James
B.S., University of Louisville, 2012

A Thesis
Submitted to the Faculty of the
University of Louisville
J.B. Speed School of Engineering
as Partial Fulfillment of the Requirements
for the Professional Degree

MASTER OF ENGINEERING

Department of Bioengineering

May 2013

PRODUCTION OF HIGH YIELD GOLD/GOLD-SULFIDE NANOPARTICLES VIA CELLULOSE MEMBRANE

Submitted by:_____
Kurtis T. James

A Thesis Approved on

_____
(Date)

by the Following Reading and Examination Committee:

_____
Robert S. Keynton, Thesis Director

_____
Andrea S. Gobin

_____
Stuart J. Williams

_____
Andre M. Gobin

ACKNOWLEDGMENTS

The author would like to thank everyone who has helped in one way or another through undergraduate and graduate school at the University of Louisville.

Dr. Andre M. Gobin

Dr. Guandong Zhang

Dr. Xinghua Sun

Dr. Robert Keynton

Dr. Martin O'Toole

Dhruvinkumar Patel

Alex Keynton

Tom Priest

Dennis Stephens

I would also like thank my family and friends who have given me enormous support throughout my academic career.

ABSTRACT

The properties of gold nanoparticles (GNP) holds promising potential for drug delivery, diagnostics, plasmonic photothermal therapy of diseases, electronics, catalysis, and photovoltaics (Liu et al., 2006; Huang et al., 2003; Thompson, 2007; Atwater and Polman, 2010). This field is growing at a fast pace with the demand for GNPs ever increasing with slow progress on development of synthesis techniques. The objective of this study was to develop a new synthesis technique that produces gold/gold sulfide (GGS) nanoparticles with a high yield. This process can control the equilibrium shift of the surface plasmon resonance (SPR) of the nanoparticles (Patel, 2012). The goal of this research is to increase the total volume of GGS nanoparticles to be synthesized while keeping their tunability for the SPR absorption peak. This research has demonstrated the ability of cellulose membrane to reduce the need for purification steps, which are associated with traditional synthesis techniques for removing small colloidal gold (<10 nm). It was found that controlling the surface area to volume ratio (SA/Vol) of the cellulose to GGS solution and temperature of the synthesis process, would provide, greater control over the SPR peak. Using these principles allows for larger volume synthesis to be performed while still retaining the ability to tune the SPR peak. It was also discovered that dialyzing out ions during the synthesis process makes bare GGS nanoparticles more stable over time. The time for the reaction to reach equilibrium was observed and showed an increase in temperature and/or SA/Vol reduces the reaction time. In conclusion, this study demonstrated how increasing the temperature and SA/Vol shifts the SPR peak and reduces the time for the reaction to reach equilibrium.

TABLE OF CONTENTS

LIST OF TABLES

LIST OF FIGURES

I. INTRODUCTION

A. Problem Statement

Over the past two decades, gold nanoparticles (GNPs) have been of great interest due to their unique physical and optical properties. The properties of GNPs hold promising potential for drug delivery, diagnostics, plasmonic photothermal therapy of diseases, electronics, catalysis, and photovoltaics (Liu et al., 2006; Huang et al., 2003; Thompson, 2007; Atwater and Polman, 2010). To date, research has focused on the application of GNPs, with slow progress on the development of new synthesis techniques, leaving a gap between research and applied technology. The desired goal for gold nanotechnology is the controlled growth of the size and shape, making GNPs robust tools. Many of the current synthesis techniques are intended for research purposes instead of industrial manufacturing. Most synthesis techniques require 24hrs to weeks to synthesize GNPs. Faster synthesis techniques have been shown to utilize a fast self-assembly process that reduces a gold salt with a sulfur group. Recently, Patel et al. (Patel, 2012) have demonstrated a new high yield synthesis process, known as “Diasynth”, which uses a cellulose dialysis membrane as a reaction vessel to control the equilibrium shift favoring the growth of the gold/gold sulfide nanoparticles (GGS). Diasynth has a reaction time of less than an hour and removes the need for purification steps (Patel, 2012). This process, however, has difficulty in scaling up with volume while keeping the tunability of the surface plasmon resonance and repeatability constant. Therefore, finer control is needed with the Diasynth process to control the growth of the particles and retain the ability to increase the total volume of the reaction.

B. Objectives

The objective of this study is to develop a new synthesis technique that produces gold/gold sulfide (GGS) nanoparticles with a high yield by evaluating the effect of temperature and surface area to volume ratio (SA/Vol) of the cellulose membrane to nanoparticle solution on the surface plasmon resonance (SPR) peak, time it takes for equilibrium to occur, the reaction environment, and GGS nanoparticle yield. The hypothesis of this study is that as the surface area to volume ratio increases, the SPR absorption peak will have a blue shift and the SPR tunability approaches a constant. Four corollaries to this hypothesis are: 1) as the reaction temperature increases the SPR absorption peak will have a blue shift; 2) as the SA/Vol ratio of cellulose membrane to nanoparticles solution increases the reaction time will decrease; 3) as the reaction temperature increases the reaction time will decrease; and, 4) the exchange of ions will affect the stability of the GGS nanoparticles.

C. Therapeutic Applications

Gold nanoparticles of are great interest in biomedicine due to their biocompatibility, ease of functionalization, stability under atmospheric conditions, and photothermal abilities (Zharov, 2006; Ghosh and Pal, 2007). Another important aspect of GNPs is their large surface to volume ratio and close size to biomolecules which allow for great opportunities in medical applications (Azzazy and Mansour, 2009). Photothermal therapy has emerged in the past decade as a promising treatment against cancer and bacteria cells. Cancer is one of the leading causes of death worldwide; in 2007, accounting for nearly 8 million deaths, and in 2030 it is projected to increase to 12 million (Bode and Dong, 2009). The need for better treatments at lower cost is in need.

Photothermal therapeutics have shown to hold promising potential in this field (Jain, Hirst, and O'Sullivan, 2012).

There is a narrow near infrared wavelength range (also known as optic or therapeutic window) from 650-900 nm where light penetrating tissue is scattered and with little absorption shown in Fig. 1. Within this window, a laser can pass through tissue with little temperature change to the surrounding tissue leaving it unharmed (Ito et al., 2000). Applying this principle with the photothermal properties of GNPs, one could heat up GNPs within the body while preventing unnecessary damage to other areas.

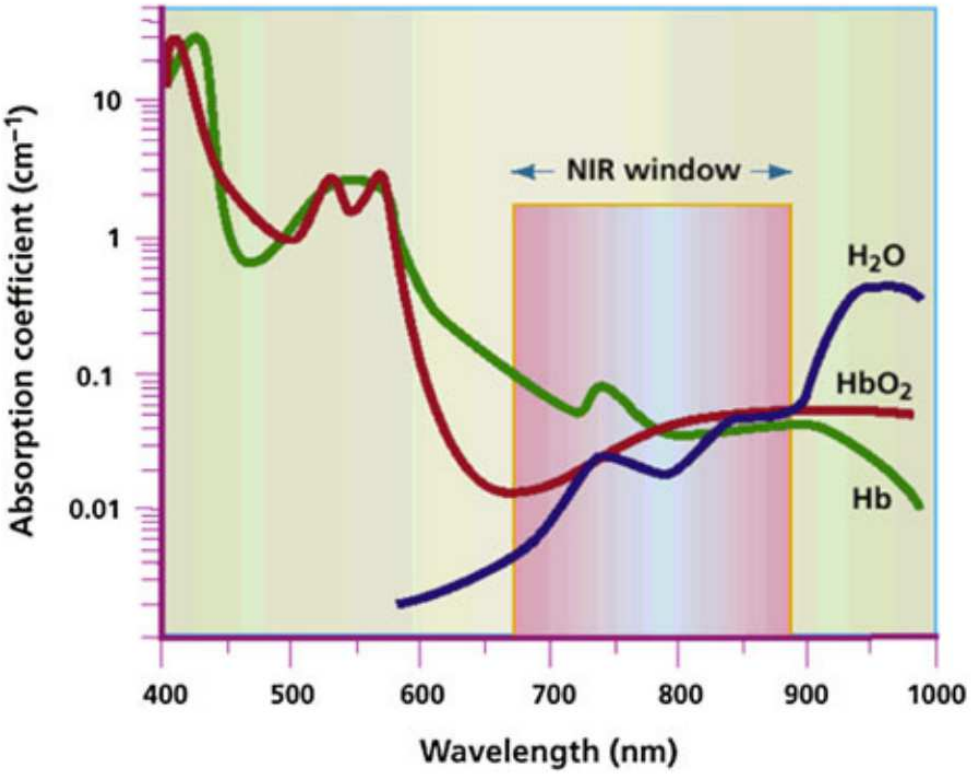

FIGURE 1 - Graph depicting the nIR window (650-900 nm) that light can pass through tissue with minimal damage at high intensities. (Weissleder, 2001).

One of the first in vivo studies to demonstrate this was by Hirsch et al. where 100 nm gold nanoshells was injected into mice tumors and a laser tuned to the SPR was

applied where the average tumor temperatures increased by 9^{o}C in control mice and 37^{o}C in nanoshell treated mice with irreversible tissue damage. All mice in the nanoshell group survived 90 days with no evidence of tumor recurrence whereas all mice in the control group were euthanized by 20 days from uncontrolled tumor growth (Hirsch et al., 2003).

Another study conducted by Gobin et al. repeated Hirschs's study with gold/gold sulfide nanoparticles. It was found that there was no difference between the two types of particles with respect to mice survival. However, the size of the gold/gold sulfide particles was 30-36 nm vs. the silica/gold nanoshell particles at 110 nm. The smaller size means that the particle has a higher absorbing cross-sectional area ratio than the gold/silica nanoshell. Also the Mie scattering theory calculations predict that the gold/gold sulfide nanoparticles will absorb 98–99% of the incident energy compared to 67–85% for the gold/silica nanoshells currently being used. The implications for these smaller, more highly energy-absorbing nanoshells for therapy are that fewer particles could be used during treatment or alternatively a lower laser power or time could be utilized during therapeutic laser administration (Gobin et al.,2010).

D. Gold Nanoparticle Morphologies

Nanoparticles are usually under 100 nm (1000 angstroms) in size and have unique properties at this dimension. Gold nanoparticles (GNPs) were first used during ancient Roman times to stain glass to various colors. The first scientific report on them wasn't observed until the 1850's by Michael Faraday (Faraday, 1857). It was not until this past century that the optical principles were understood in more detail. It is now known that nanoparticles are larger than individual atoms but are smaller than the bulk solid, making

materials at the nanoscale exhibit behavior intermediate between a macroscopic solid and an atomic system (Gosh and Pal, 2007). This allows for GNPs to have unique optical and electronic properties capable of being determined by their size and shape (Link and El-Sayed, 1999b). Some of the optical properties for GNPs include surface plasmon resonance (SPR), surface enhanced Raman scattering (SERS), nonlinear optical properties (NLO), and luminescence making GNPs a robust tool (Klar et al. 1998; Averitt et al. 1999; Cao et al. 2002). Along with its optical properties, GNPs can be irradiated by a laser at a wavelength around the SPR band which can efficiently convert the photon energy to thermal energy (Zharov, 2006).

1. Surface Plasmon Resonance

A unique optical characteristic of gold nanoparticles, which is an important topic within this study, is surface plasmon resonance (SPR). This phenomenon is present within many metal nanoparticles, including the GNPs described herein. Figure 2 illustrates the principles behind SPR with light (Willets and Van Duyne, 2007). SPR is created in metallic nanoparticles from the interaction of electromagnetic radiation with the metal sphere. A dipole is induced, which oscillates in phase with the electric field of the incident electromagnetic radiation. This causes the conduction electrons in the particle to act like an oscillator system (Ghosh and Pal, 2007).

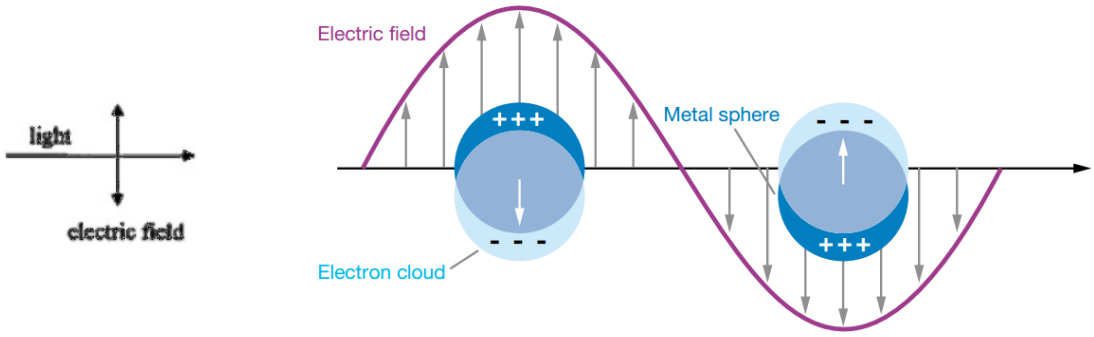

FIGURE 2 - Illustration showing a localized surface plasmon. (Willets and Van Duyne, 2007).

2. Nanospheres

Gold nanospheres (also known as gold colloids) range from less than a nanometer to over 100 nm in diameter and are synthesized by a controlled reduction of an aqueous $HAuCl_4$ solution with a reducing agent. One of the most commonly used reducing agents is citrate, which can produce nearly monodisperse gold nanospheres (Turkevich et al 1951; Frens 1973). The size of the nanospheres can be controlled by varying the citrate/gold ratio. Generally, a smaller amount of citrate will yield larger nanospheres. These particles have a strong absorbance peak in the visible range typically from 520 to 540 nm as shown in Figure 3a (Link and El-Sayed, 1999b). The major limitations of this method are the low yield and the restriction of using water as the solvent (Cai et al., 2008).

3. Nanorods

In preparing gold nanorods (GNRs) there are two different approaches available: 1) electrochemical; and, 2) seed-mediated (Yu et al., 1997; Nikoobakht and El-Sayed, 2003). When the shape of the gold nanoparticles is changed from sphere to rod, the SPR spectrum splits into two peaks; a stronger, long-wavelength band in the nIR region is due to the longitudinal oscillation of electrons while a weaker short-wavelength band in the

visible region (around 520 nm) is due to the transverse electronic oscillation (Link and El-Sayed, 1999a). Unlike gold nanospheres, the absorption spectrum of the gold nanorods is very sensitive to the aspect ratio (length/width). With an increase in the nanorod aspect ratio, the SPR absorption peak of the longitudinal band significantly shifts redshifts to the red region of the spectrum (Huang et al., 2008). Figure 3b shows a TEM of GNRs and their spectra profile.

4. Nanoshells

Oldenburg et al. (Oldenburg et al., 1999) developed a gold nanoshell structure, which is composed of a silica dielectric core (100–200 nm in diameter) surrounded by a thin layer of gold shell (5–20 nm). The nanoshells absorb and scatter strongly in the nIR region. The SPR of the nanoshells can be tuned by adjusting the ratio of the thickness of the gold shell to the diameter of the silica core. A redshift of the SPR wavelength occurs with a decrease in the thickness to diameter ratio (Loo et al., 2004; Huang et al. 2008). Mie theory uses Maxwell's equations that can be used to estimate the nIR spectra profile of gold nanoshells (Mie, 1908; Gosh and Pal, 2007). These particles require a multiple step synthesis process, but result in a monodispersed homogenous population. Figure 3c, shows a TEM of gold nanoshells and their respective spectra as well.

5. Nanoprisms

A variety of synthesis routes have been used to generate triangular, plate-like nanostructures (also referred to as nanoprisms, nanotriangles, nanoplates, or nanodisks) (Millstone et al., 2009). In particular, these prisms have SPRs that are tunable throughout the visible and nIR regions of the spectrum by controlling the nanoprism's edge length,

thickness, and tip morphology (Young et al., 2012). Gold nanoprism synthesis typically generates gold colloid and requires purification steps to acquire a homogenous solution (Young et al. 2012). Figure 3d shows a TEM image and spectra profile of gold nanoprisms.

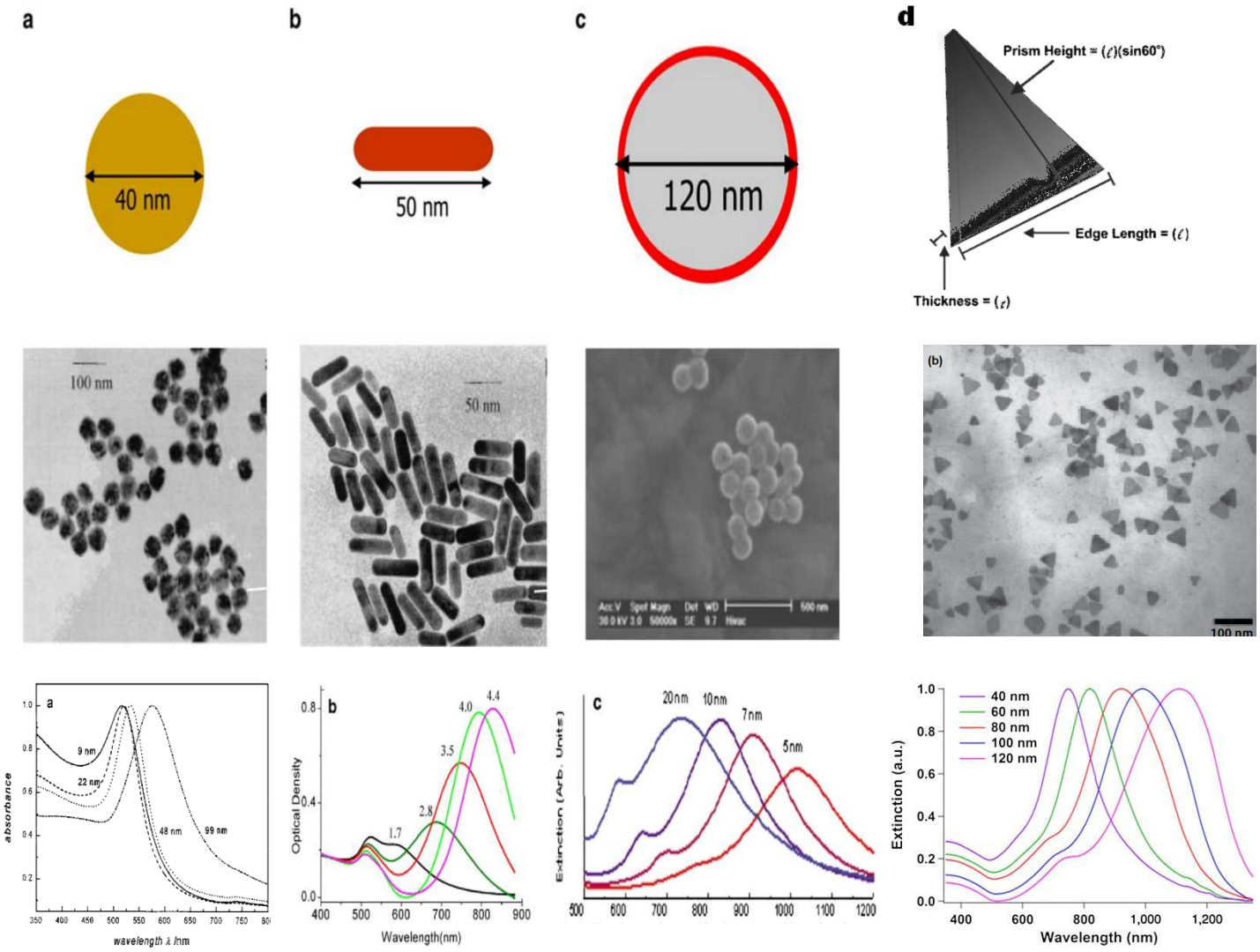

FIGURE 3 - (a) Top - Illustration of colloidal gold nanoparticle (Huang et al., 2008), Middle - TEM image of 99 nm gold nanoparticles (Link and El-Sayed, 1999b), Bottom - UV-vis absorption spectra of various diameter gold nanospheres (Link and El-Sayed, 1999b). (b) Top - Illustration of gold nanorod (Huang et al., 2008), Middle - TEM image of 50 nm gold nanorods (Link and El-Sayed, 1999a), Bottom - UV-vis optical density spectra of gold nanorods of various lengths (Nikoobakht and El-Sayed, 2003; Huang et al., 2008), (c) Top - Illustration of silica core/gold nanoshell (Huang et al., 2008), Middle - TEM image of silica core/gold nanoshell particle (Loo et al., 2004), Bottom - UV-vis extinction spectra of various shell thickness of silica core/gold nanoshell (Oldenburg et al., 1999; Huang et al. 2008), (d) Top-Illustration of gold nanoprism (Millstone et al., 2009), Middle - TEM image of gold nanoprisms (Tréguer-Delapierre et al., 2008) Bottom-UV-vis extinction spectra for gold nanoprisms of varying edge lengths (Young et al. 2012).

6. Gold/Gold Sulfide Nanoparticles

Gold/Gold nanoparticles (GGS) are synthesized by reacting sodium sulfide (Na_2S) or sodium thiosulfate ($Na_2S_2O_3$) with a gold salt, tetrachloroauric acid ($HAuCl_4$), in a traditional one-step or two-step method. Below, Eq. 1 and 2 shows the reaction for both Na_2S and $Na_2S_2O_3$ respectively (Averitt, Sarkar, and Halas, 1997; Schwartzberg, 2007; Patel, 2012).

$$HAuCl_4*4H_2O + Na_2S*9H_2O = Au_2S + Au + Au_2S/Au\ (\text{nanoshell}) + S^+ \quad (1)$$

$$HAuCl_4*3H_2O + Na_2S_2O_3*5H_2O = Au_2S + Au + Au_2S/Au\ (\text{nanoshell}) + S^+ + H^+ + SO_4^{2-} + NaCl + SO_3^{2-} + S_2O_6^{2-} + Cl^- + Na^+ \quad (2)$$

The advantage of these particles is their ability to be synthesized without the assistance of additional templates, capping reagents, or seeds in addition to having a strong tunable SPR absorption peak in the nIR range (Zhang et al., 2012). These self-assembling particles require one or two steps and can be synthesized in less than an hour. This synthesis process also has associated issues, mainly the control over the formation of the particle structure and a high concentration of small colloidal gold (<10 nm nanospheres) formed as a result of the self-assembly process (Schwartzberg et al. 2007). The traditional one-step reaction calls for the mixing of 2mM $HAuCl_4$ with 1mM Na_2S

solution at a volumetric ratio of 1:2, while stirring at room temperature (Diao and Chen, 2006). For the two-step method, Na_2S is mixed with $HAuCl_4$ for a few minutes and then an additional amount of Na_2S is added (Zhou, Honma, and Komiyama, 1994). The two-step becomes more difficult to repeat with increasing the total volume of the reaction. This study will focus on the one-step method over the two-step to ensure repeatability. Both methods produce a heterogeneous mixture of nanoparticles containing gold colloid, spheroids, triangular plates, and rods. Mie theory cannot be applied to these particles since they are not homogenous spherical particles (Gosh and Pal, 2007). The SPR peak can be tuned to a certain wavelength by adjusting the molar ratio of Na_2S or $Na_2S_2O_3$ and $HAuCl_4$ (Zhou, Honma, and Komiyama, 1994; Zhang et al., 2012; Diao and Chen, 2006; Schwartzberg et al. 2007). Fig. 4 shows the tunability of the SPR peak in a one-step process by varying the molar ratio (Zhang et al., 2012).

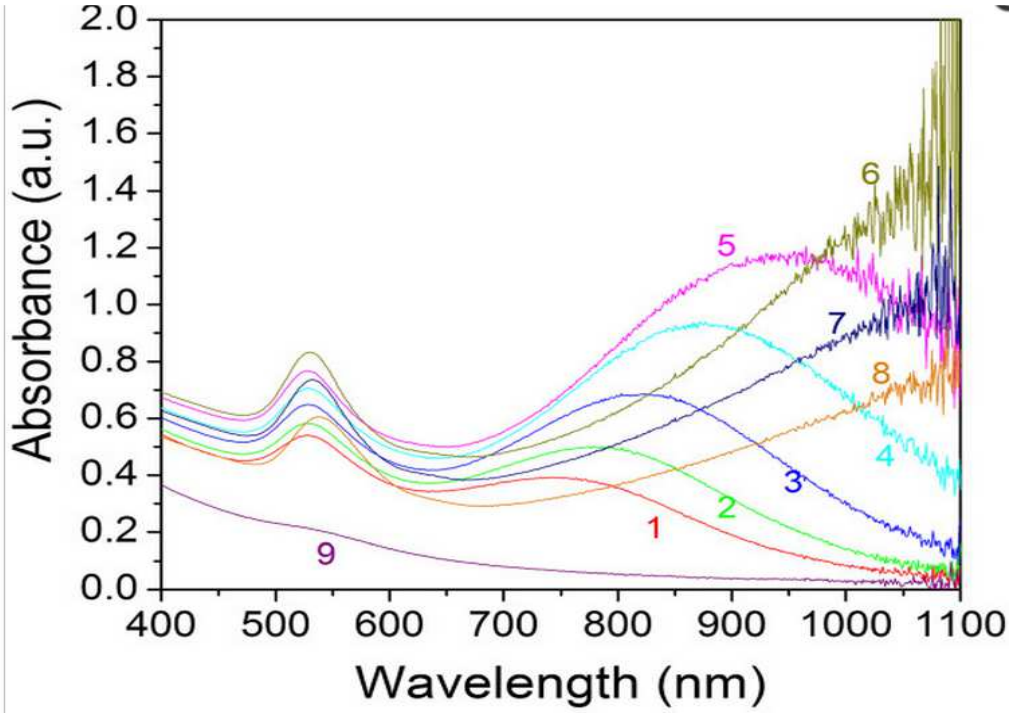

FIGURE 4 - Optical spectra of GGS nanoparticles from a traditional one step method with different molar ratios, $Na_2S_2O_3$:$HAuCl_4$. (Zhang et al., 2012)

The traditional one-step synthesis process forms a high concentration of small colloidal gold particles (<10 nm) as evidenced by the 530 nm peak absorption and the nIR peak varies depending on the molar ratio. Fig. 5 shows the UV-vis-nIR spectra of GGS manufactured via traditional one-step synthesis (black) and purified (blue) (Zhang et al., 2012). After purification from centrifugation, the resulting solution's nIR SPR redshifts and reduces the colloidal gold as illustrated by the reduction in peak absorbance at 530 nm (Figure 5 blue). The removal of the small colloidal gold was not only evident from the 530 nm absorbance peak drop in Fig. 5, but can also be seen from transmission electron microscopy (TEM) image shown in Figs. 6 and 7 (Patel, 2012; Zhang et al., 2012).

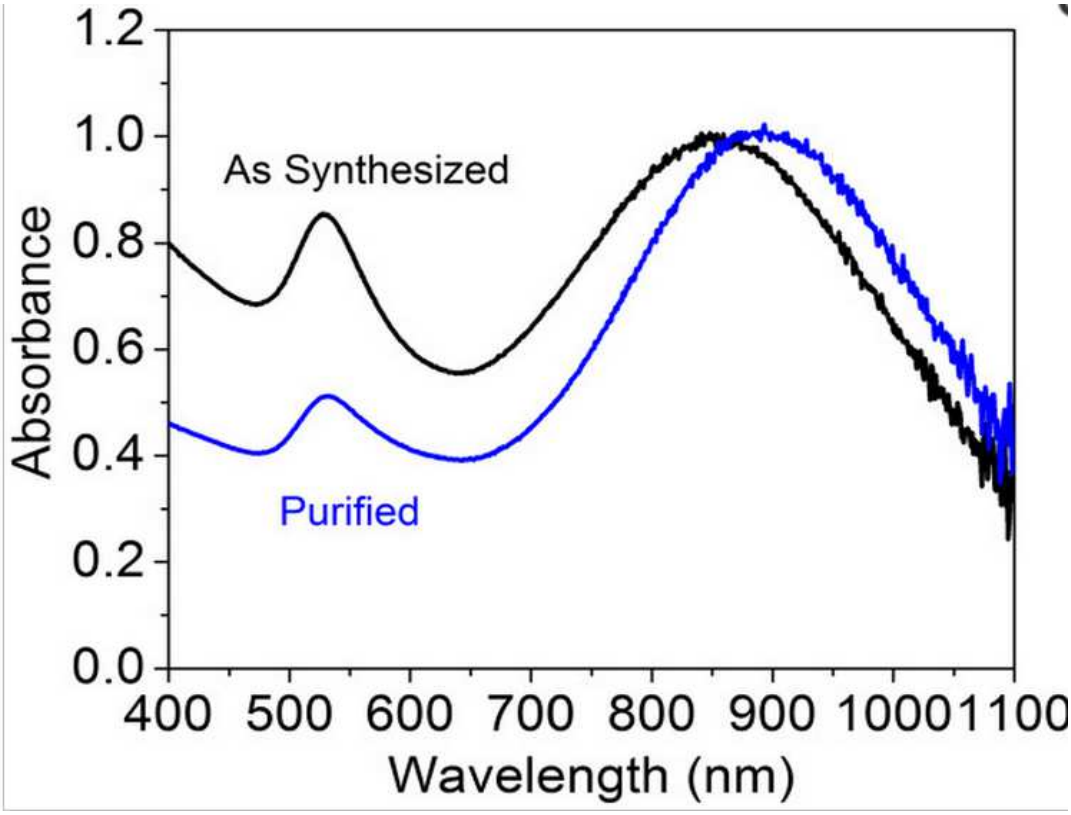

FIGURE 5 - UV–vis-nIR spectra of GGS nanoparticles shown before and after purification via centrifugation. The sample is separated at 1,000×g for 20min. (Zhang et al., 2012)

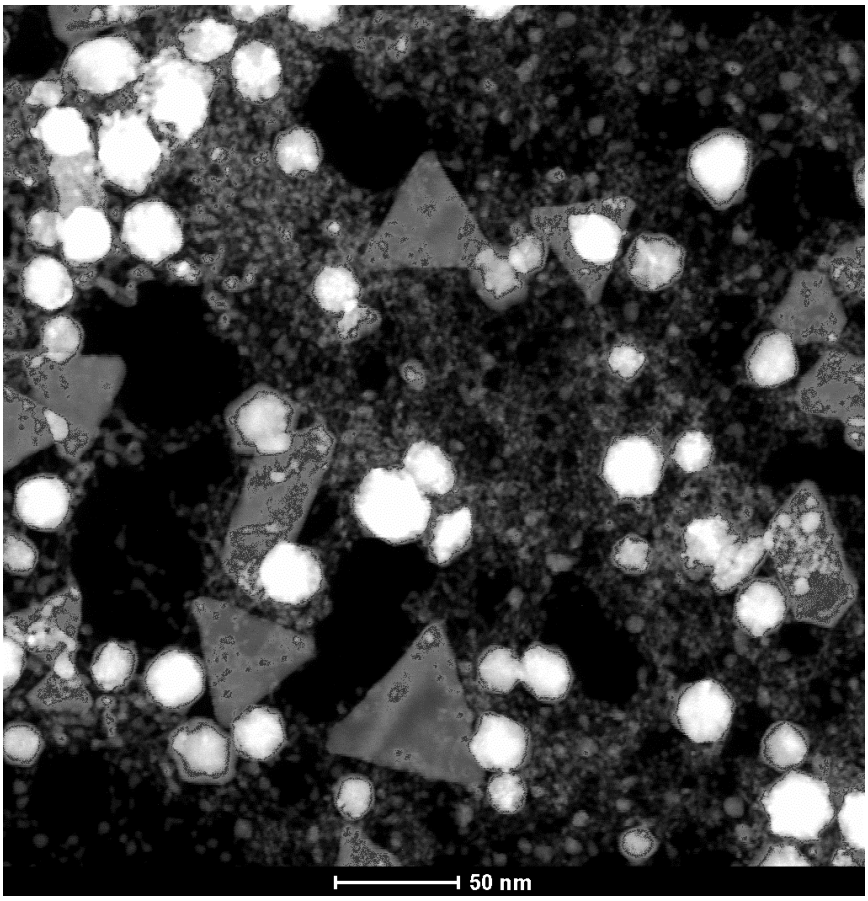

FIGURE 6 - TEM image of gold/gold sulfide nanoparticles made with traditional one step synthesis. (Patel, 2012)

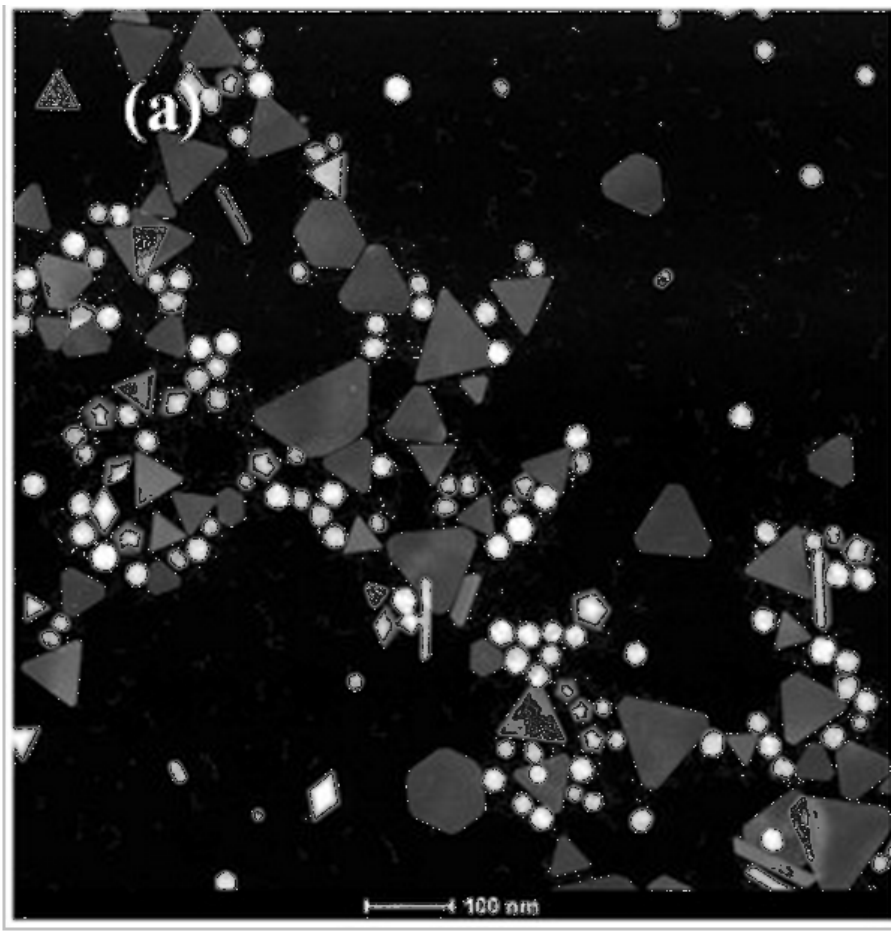

FIGURE 7 - TEM image of GGS nanoparticles after centrifugation to remove gold colloid. (Zhang et al., 2012)

7. Diasynth

The Diasynth process was described by Patel (Patel et al., 2012) as an exchange of ions and GNPs which occurs between the GGS solution and surrounding deionized (DI) water via a cellulose membrane resulting in an equilibrium shift that changes the SPR nIR peak position. From Eq. (2), there are many ions present from the reaction that can affect the growth of the GGS particles, thereby altering the SPR peak equilibrium shift. Patel (Patel et al., 2012) tested different molecular weight cutoffs (MWCO) and various molar ratios of reactants to determine the optimal conditions for a high absorbance peak centered on 820 nm, while minimizing the colloidal gold concentration (530 nm peak). It was seen that different MWCOs would alter the equilibrium shift due to the different rates of diffusion for the exchange ions and GNPs. Fig. 8 shows the change in colors in the traditional synthesis (A-D) vs. Diasynth (E-H) over an hour time span.

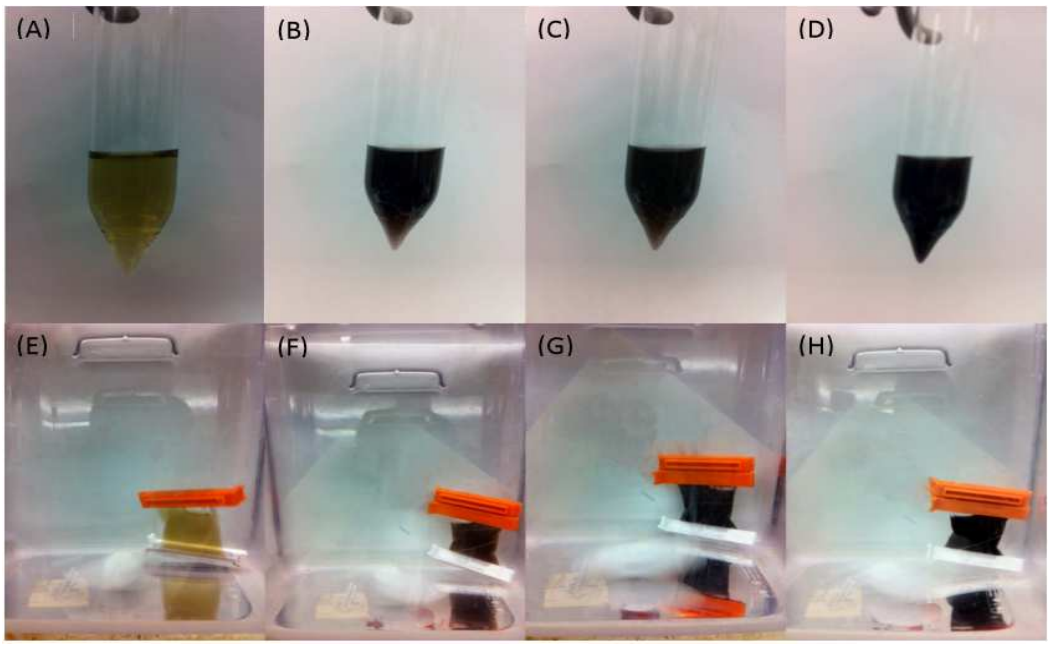

FIGURE 8 - Image of Non-Dialysis synthesis and dialyzed synthesis over 1hr time period: (A) 30sec, (B) 5 mins, (C) 30mins, (D) 1hr. Image of Diaylzed sample over 1hr time period: (E) 30sec, (F) 5 mins, (G) 30mins, (H) 1hr. (Patel, 2012)

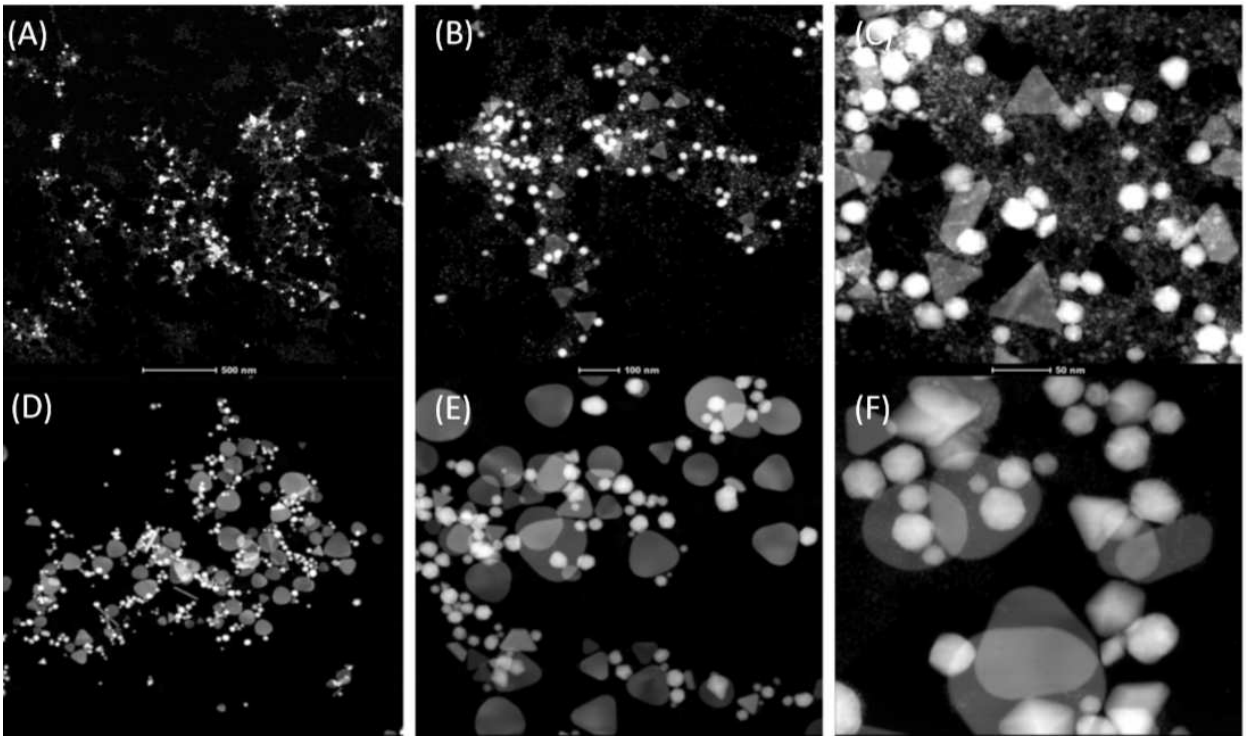

FIGURE 9 - TEM images of traditional synthesis (A-C) and Diasynth (D-F).
(Patel, 2012)

The Diasynth process (Fig. 9) was shown to be just as effective at removing colloidal gold as the centrifugation method of the traditional GGS synthesis process (Fig. 7). From Patel, it was seen that the Diasynth is a high yield synthesis process for GGS nanoparticles.

8. Cellulose

Porous materials have been used as nanoreactors for metal nanoparticle synthesis. Specifically Ag, Au, Pt, and P nanoparticles have been synthesized in porous cellulose (He, Kunitake, and Nakao, 2003). He et al. (2003) submerged porous cellulose fibers in 10mM $AuCl_3$, then added $NaBH_4$ (reducing agent) and saw the clear membrane change color to a light pink. Fig. 10 shows a TEM image and size distribution histogram from their findings.

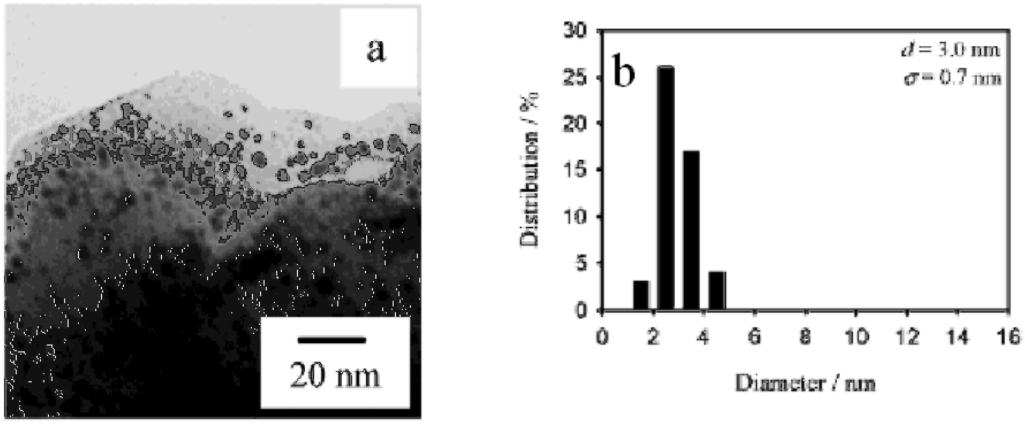

FIGURE 10 - (a) TEM image and (b) histogram of Au nanoparticles in cellulose fiber. (He, Kunitake, and Nakao, 2003)

The metal ions are impregnated into and reduced onto the cellulose fibers in the presence of a reducing agent. This method can be employed without the addition of a reducing agent, because adsorption of metal ions on the cellulose fibers may be reduced to metal nanoparticles by organic moieties such as terminal aldehyde or carboxylic groups. The structure and the presence of ether and hydroxyl groups in cellulose fibers create an effective nanoreactor for synthesis of the metal nanoparticles. The ether oxygen and the hydroxyl group not only anchor metal ions tightly onto cellulose fibers via ion-dipole interactions, but also stabilize metal nanoparticles by strong bonding interaction with their surface interactions (He, Kunitake, and Nakao, 2003; Pinto and Neves, 2012, 77).

II. MATERIALS AND METHODS

A. Instrumentation

UV absorption spectrum was measured on all samples at a 10x dilution in water with the Varian Cary 50 BIO UV Visible Spectrometer. The size and zeta potential measurements were measured at a 10x dilution in DI water on the Malvern Zetasizer Nano ZS90. It is important to note that the size measured is the hydrodynamic radius with the Malvern Zetasizer. The conductance measurements were performed with the Brookhaven Zeta Pals instrument. The scanning tunneling electron microscopy (STEM) was performed on the Zeiss SUPRA FE-SEM. The statistical analysis was performed with Minitab software. Image j software was used to measure the size and counts for the size distribution analysis.

B. Reactants

The gold salt used for all experiments was hydrogen tetrachloroaurate(III) trihydrate ($HAuCl_4*3H_2O$) purchased from Alfa Aesar. A 2mM solution is prepared with DI water and protected from light with aluminum foil. The sulfur used in all experiments was sodium thiosulfate pentahydrate ($Na_2S_2O_3*5H_2O$) purchased from Sigma-Aldrich.

C. Cellulose Membrane

The cellulose dialysis tubing was stored at 4^oC and pretreated by soaking in 2L of DI water for 4 days while changing the water every day to remove preservatives (glycerol, sodium azide, and/or sulfur in trace amounts). Once hydrated, the membrane was kept in 2L of DI water. Before use, the membrane was cut to desired lengths and rinsed thoroughly inside and out with running DI for 3-5 minutes. The 8 (FW 50mm;

Spectra/Por 7), 15 (FW 45mm; Spectra/Por 7), and 12-14kDa (FW 120mm; Spectra/Por 2) molecular weight cutoff (MWCO) cellulose membranes were purchased from Spectrum Labs and 12kDa (FW 43 and 76mm) from Sigma-Aldrich.

D. Traditional Synthesis

For the traditional synthesis procedure, 3mM $Na_2S_2O_3$ was added to 2mM $HAuCl_4$. The molar ratio of the two reactants controlled the size and placement of the SPR nIR peak. Traditional synthesis protocol consisted of measuring 150ml of 2mM $HAuCl_4$ into a 250ml polystyrene 75cm^2 canted neck flask (Corning), then adding 62ml of 3mM $Na_2S_2O_3$ into the polystyrene flask, agitating for 1 minute and letting sit for 45 minutes. The solution was aliquoted into eight 50ml centrifuge test tubes (VWR) and centrifuged three times at 1,000g for 20min, collecting the pellet each time to purify sample.

E. Diasynth

This method used the dialyzing role of the dialysis membrane to exchange ions and small gold nanoparticles during synthesis with the surrounding water. The protocol for this process requires a 177-203 mm length of 12kDa MWCO cellulose dialysis tubing (Flat Width 43mm, Sigma Aldrich). One end of the dialysis tubing was clipped with a weighted dialysis clip and 44ml of 2mM $HAuCl_4$ was added into the membrane through the open end of the dialysis tubing. 10ml of 3mM $Na_2S_2O_3$ was added into the solution via mechanical pipette with continued mixing of the solution by bubble mixing through the mechanical pipette for 10 seconds. Subsequently, the other end of the membrane was clipped and air was removed from the tubing. The tubing was placed in 7L of 25^oC DI

water with a stir bar and allowed to react for 60 min. After synthesis, the GGS nanoparticle solution was stored in 50ml test tubes at room temperature.

F. Reactor

To ensure reproducibility of the GGS nanoparticles and scale up of the synthesis volume, a reactor was constructed out of glass. Glass was chosen because it does not react readily with gold. The reactor consisted of a 61cm tall cylinder with an inner diameter of 10cm (Fig. 11a). An inlet and outlet was at the top and bottom, respectively, of the reactor for DI water circulation. A glass membrane frame was made 37cm high with a 7cm outer diameter to hold open the membrane whereas still maximizing the surface area for diffusion, shown in Fig. 11b. The top of the glass membrane frame had a diameter of 13cm so the rest of the frame could be inserted into the reactor while held suspended at the top. A glass stir rod was made for the length of the membrane frame for stirring the solution.

The membrane was placed over top of the membrane frame, tied in a knot at the bottom and zip-tied at the top to secure the membrane overtop the frame. Once the membrane was secured, it is placed within the reactor and then circulation of DI water can begun (Neslab RTE 221 refrigerated bath/circulator). The two reactants were then added into the membrane with the stir rod for mixing (Heidolph RZR 2021).

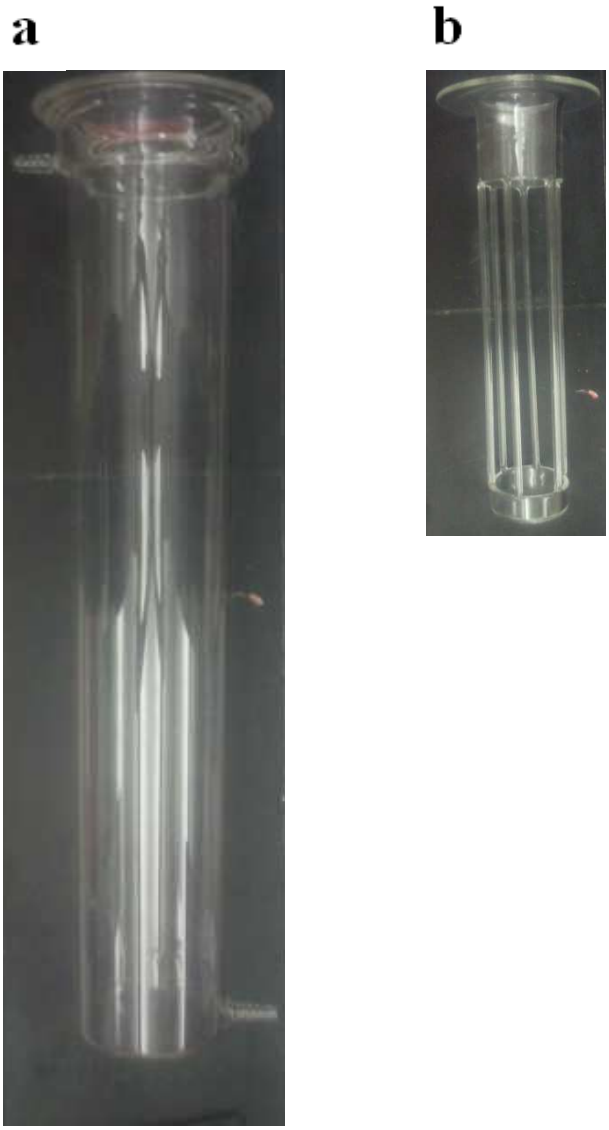

FIGURE 11 – (a) Glass reactor that has inlet and outlet at top and bottom and (b) glass membrane frame that is placed inside of reactor.

G. Experiments

1. Experiment A

To verify that ions and small particles were being dialyzed out of solution during the Diasynth process, a conductance experiment was performed on the dialysate. A

sample was made with the Diasynth process: 8ml of 3mM $Na_2S_2O_3$ was added to 44ml of 2mM $HAuCl_4$ inside a 152mm long 12kDa cellulose membrane (76mm Flat Width) and placed in 7L of 25^oC DI water inside a square plastic 8L tub with constant stirring. 1.8ml of dialysate was collected between half the distance from the cellulose membrane to container wall. The conductance was measured at 0, 1, 10, 20, 30, 40, 50, and 60 minute time intervals. This same experiment was performed with 52ml of DI water within the membrane as a control.

2. Experiment B

This experiment used the same principles as Patel to perform the Diasynth process on a total volume batch of 216ml. This was the largest volume synthesis, to date: 40ml of 3mM $Na_2S_2O_3$ was added to 176ml of 2mM $HAuCl_4$ inside a 12kDa cellulose membrane (43mm Flat Width) and placed in 55L of DI water inside a plastic 113L tub with constant stirring with a magnetic stir bar. The dialysis clips used were weighted on both ends. A magnet was used on the outside of the tub to hold the membrane horizontally across for a uniform distribution of solution across the membrane as seen in Fig. 12. Two different SA/Vol ratios were used to test their effect on the SPR nIR peak: 150 (375mm; sample M7) and 240mm^2/ml (600mm; sample M8).

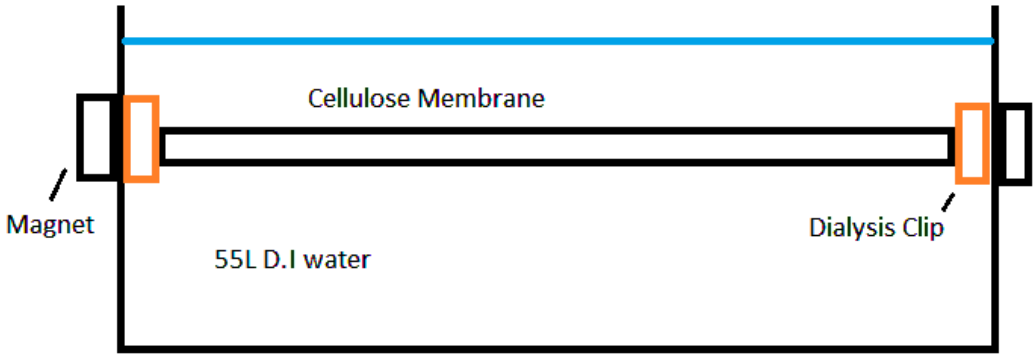

FIGURE 12 – Schematic depicting the Diasynth setup for a 216ml volume batch.

3. Experiment C

This experiment was the first time the new reactor configuration was used and a reaction synthesis volume of 746ml was produced. A 45cm long 12-14kDa (145mm^2/ml; 120mm Flat Width) membrane was placed overtop the glass membrane frame and tied above and below with zip ties. 608ml of 2mM $HAuCl_4$ was mixed with 138ml of 3mM $Na_2S_2O_3$ simultaneously while pouring into the membrane. Stirring occurred at 100rpm. Since the SA/Vol ratio was low, it was expected that a redshift would occur on the SPR absorption. It was theorized that constant stirring would increase the exchange of ions to cause a blue shift, offsetting the redshift caused from low SA/Vol. Constant DI water circulation occurred at a rate of 15L/min. The reaction lasted for 60min before storing in a 1 L glass bottle and the UV-spectrum absorption measured.

4. Experiment D

This experiment was performed to determine if either of the reactants reacted with the cellulose membrane during the Diasyth process. 20 ml of 3 mM $Na_2S_2O_3$ was placed inside a 5 cm long 8, 12, and 15 kDa membrane in 7 L of DI water for 2 hours. The same procedure was followed for 32 ml of 2 mM $HAuCl_4$ poured inside the membranes under the same conditions.

5. Experiment E

This experiment was performed to determine the effects of the cellulose membrane on the SPR nIR peak. 32.6ml of 2mM $HAuCl_4$ was placed into 50ml centrifuge test tube. The cellulose membrane was cut to the desired length that corresponded to surface area to volume (SA/Vol) ratio and rinsed thoroughly with DI water. It is then placed inside the test tube along with the $HAuCl_4$ solution. 7.4ml of 3mM $Na_2S_2O_3$ was added to the solution via mechanical pipette and bubble mixed for 10 seconds at room temperature. The cap of the test tube was screwed on and the test tube was rocked back and forth by hand for 1 min. The sample was allowed to react at room temperature for 60 min before measuring the sample's UV-spectrum absorption. An n=3 was performed for each SA/Vol ratio: 0, 320, 650, and 1075mm^2/ml. An analysis of variance (ANOVA) was performed to confirm the significance.

6. Experiment F

An experiment was performed to determine the effects of a dry Diasynth (no DI water) method on the equilibrium shift of SPR nIR peak. The cellulose membrane was used as the reaction vessel with no DI water present for dialysis. 40ml of 3mM $Na_2S_2O_3$

was added to 176ml of 2mM $HAuCl_4$ inside a 508mm (360mm^2/ml; sample M17) and 250mm long (175mm^2/ml; sample M18) 12kDa cellulose membrane (76mm Flat Width) and placed flat inside a plastic 113L tub. The reaction lasted for 60min at room temperature.

7. Experiment G

This experiment was performed to determine the effects of temperature and SA/Vol of the cellulose membrane to GGS solution has on the SPR nIR peak during Diasynth. 7.4ml of 3mM $Na_2S_2O_3$ was added to 32.6ml of 2mM $HAuCl_4$ inside a 100 (220mm^2/ml), 150 (340mm^2/ml), or 200mm long (470mm^2/ml) 12kDa cellulose membrane (43mm Flat Width) and placed in 2L of DI water at 25, 37, or 50^{o}C. An n=3 was performed for an ANOVA. Measurements were taken at 10min intervals to determine the reaction equilibrium kinetics. The GGS nanoparticle solution for each sample was stored in 50ml centrifuge test tubes at room temperature and size and UV-spectrum absorption was measured 14 days after the reaction to test the stability of the particles.

8. Experiment H

Experiment H was similar to Experiment E, except the Diasnyth process was performed in the absence of DI water and different temperatures were investigated. This experiment was performed to determine the effects that the cellulose membrane has on the GGS SPR nIR peak during Diasynth when temperature and SA/Vol ratio were varied. 7.4ml of 3mM $Na_2S_2O_3$ was added to 32.6ml of 2mM $HAuCl_4$ inside a 100 (220mm^2/ml), 150 (340mm^2/ml), and 200mm long (470mm^2/ml) 12 kDa cellulose

membrane (43mm Flat Width) and placed in 2L of DI water at 25, 50, and 100^{o}C. An n=3 was performed for an ANOVA. UV-spectrum absorption measurements were taken at 10min intervals to determine the reaction equilibrium kinetics. The GGS nanoparticle solution for each sample was stored in 50ml centrifuge test tubes at room temperature and the size and UV-spectrum absorption was measured 14 days after the reaction to test the stability of the particles.

9. Experiment I

For Experiment I, scanning tunneling electron microcopy (STEM) will be performed on two different samples that have a SPR nIR peak near 800 and 900nm. The size of the samples will be measured and counted with Imagej software manually. This experiment will determine the size distribution between the two samples.

III. RESULTS AND DISCUSSION

A. Experiment A

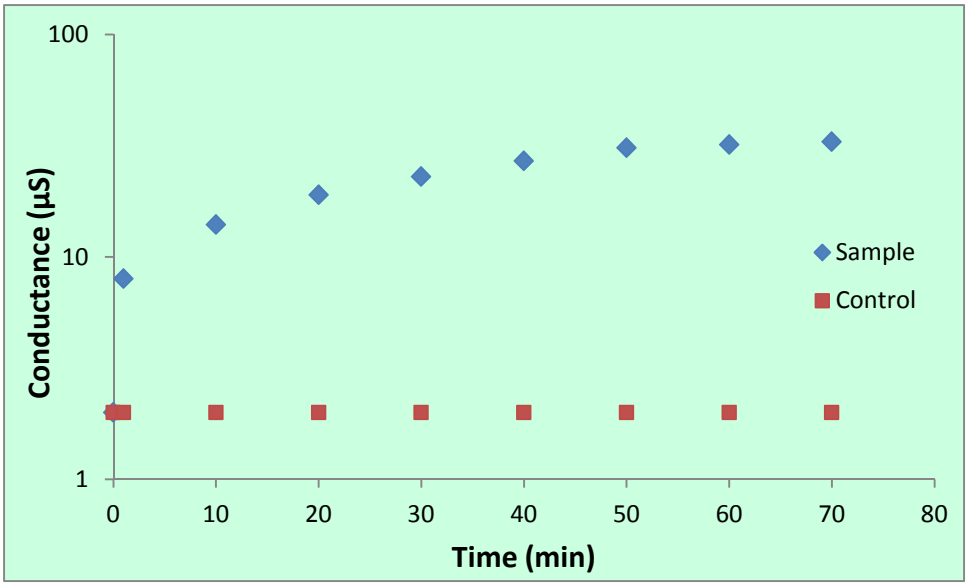

FIGURE 13 - Conductance vs. time for GGS sample dialysate (blue) and DI water control (red).

TABLE I

CONDUCTANCE OVER TIME

Sample		Control	
min	µS	min	µS
0	2	0	2
1	8	1	2
10	14	10	2
20	19	20	2
30	23	30	2
40	27	40	2
50	31	50	2
60	32	60	2
70	33	70	2

The conductance over time for the GGS sample shows in Fig. 13 and Table I, that there are ions and/or gold nanoparticles within the dialysate. The increase in conductance

over time in the dialysate is evidence that there is diffusion through the membrane. The control (DI water) shows that no change in conductance occurs over time, proving that the cellulose membrane or the dialysis clips are not attributing to the conductance measurements. The conductance measurements increase steadily until 50 min when it began to plateau at 31µS which marks the reaction reaching the equilibrium point.

B. Experiment B

The GGS solution was collected after the reaction (60min) and a UV-spectra profile was measured at 10x dilution in water. The results are shown below in Table II and Fig. 14. This experiment shows promising results for the capability of scaling up the reaction volume during synthesis while keeping the tunability of the SPR nIR peak constant by altering the SA/Vol ratio. This represents the largest synthesis, to date since Patel performed his Diasynth process under the same conditions, but with a maximum volume of 50ml. The blue shift of the SPR nIR due to increasing the SA/Vol ratio proves the hypothesis. This blueshift could be due to an increased diffusion rate or an interaction between the GGS and the cellulose membrane at the higher SA/Vol ratios.

TABLE II

EXPERIMENT B GGS SAMPLE PROPERTIES

SA/Vol (mm^2/ml)	nIR Peak (nm)	Optical Density	Size (nm)	Zeta Potential (mV)
150	920	8.6	84.27	-28.25
240	810	7.1	63.21	-29.9

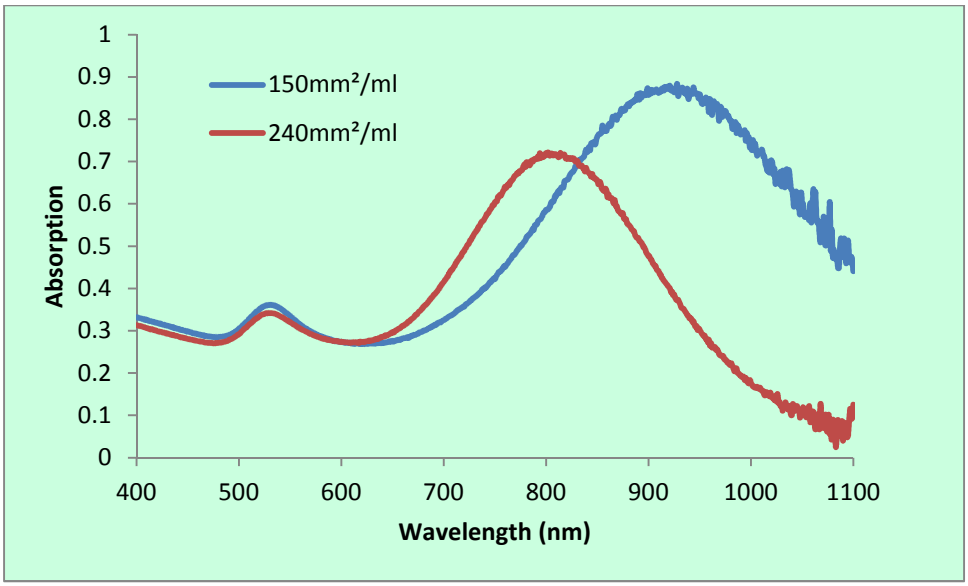

FIGURE 14 – The UV-spectra of gold/gold sulfide nanoparticles synthesized with Diasynth with a total volume of 216ml. Measured with two different SA/Vol ratios: 150mm^2/ml (blue curve) and 240mm^2/ml (red curve).

C. Experiment C

The GGS solution was collected after the reaction (60min) and a UV-spectra profile was measured at 10x dilution in water. The results are shown below in Table III and Fig. 15. The stirring does not shift the SPR nIR peak as originally thought. We theorized that the stirring would increase exchange of ions and/or small gold nanoparticles out of solution and into the DI water space, which would then cause a blue shift in SPR nIR peak equilibrium to accommodate for the decrease in the SA/Vol ratio. The Day 0 SPR nIR peak is above 1100 nm and shifts towards the blue spectrum (940 nm) by Day 3, which the shift in equilibrium is not reached on Day 0, but has reached it by Day 3. Another measurement was performed at Day 5 with no significant difference from Day 3. The SPR nIR peak on Day 3 is broad indicating a varied size distribution from poor particle formation which could be the result of active mixing instead of passive diffusion for ion exchange. Another possibility would be that the low SA/Vol ratio

(145mm^2/ml) had a resdshift on the SPR absorption peak not because of poor ion exchange, but from the decrease in cellulose present during the reaction.

TABLE III

EXPERIMENT C GGS SAMPLE PROPERTIES

Day	nIR Peak (nm)	Optical Density	DLS Size (nm)	Zeta Potential (mV)
0	>1100	7.0	NA	NA
3	940	4.5	63.52	NA

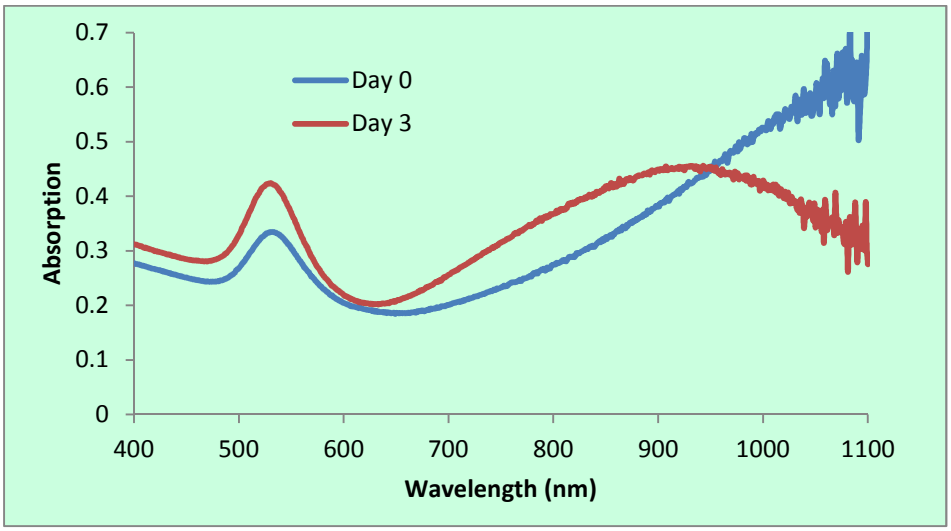

FIGURE 15 – The UV-spectra of gold/gold sulfide nanoparticles synthesized within the reactor with a total volume of 746ml. Measured at Day 0 (blue curve) and Day 3 (red curve).

D. Experiment D

The $Na_2S_2O_3$ shows to have no effect on the change in color on the cellulose membrane for 8, 12, and 15kDa MWCO. The $HAuCl_4$ did show signs of reacting with the cellulose membrane as shown in Fig. 16. The 12kDa membrane seems to have had a

stronger reaction with $HAuCl_4$ than the 8 or 15kDa membranes from the deeper pink/purple color. This is mostly likely due to trace amounts of sulfur compounds present on the 12kDa membrane acting as a reducing agent. The other two membranes are purchased from another vendor and do not contain the sulfur compounds. This experiment does show visually some interaction between $HAuCl_4$ and the cellulose membrane. The 8kDa membrane displays a light pink, 12kDa membrane displays a deep pink/purple, and the 15kDa membrane displays a pink/blue color. These results are similar to the findings of He et al. (He, Kunitake, and Nakao, 2003). The cellulose membrane uptakes the gold ions and entraps them within the cellulose fibers. In He's study, the gold ions are being reduced and retained. Scanning electron microscopy (SEM) is needed to confirm that gold nanoparticles are being reduced on the cellulose fibers.

FIGURE 16 – Image of 8 (left), 12 (middle), and 15kDa (right) cellulose membranes in the presence of $HAuCl_4$

E. Experiment: E

This experiment shows the effect of the SA/Vol ratio of the cellulose membrane to GGS nanoparticle solution has on SPR nIR peak. As shown in Fig. 17 and 18, the

higher the SA/Vol ratio, the more the nIR peak has a blue shift. The trend shows an asymptotic decay that approaching the wavelength of 800nm. The error bars are the standard deviation for an n=3 for each data point. Since there is no dialysis occurring in this experiment, the equilibrium shift seen must be from the reaction with the cellulose membrane. The decrease in the 530 nm absorption peak from the traditional synthesis process may be from the cellulose membrane retaining the gold colloid. Table IV summarizes the results of the experiment.

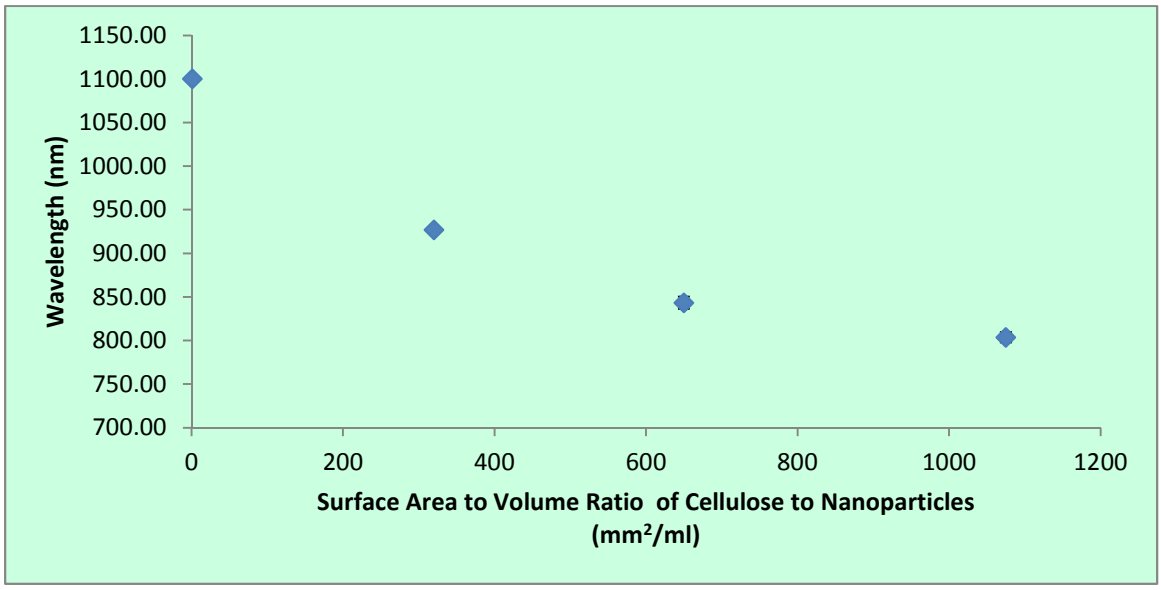

FIGURE 17 - SA/Vol ratio of cellulose membrane to nanoparticle solution vs. SPR nIR peak position for traditional synthesis in 50ml test tube reacted in presence of cellulose membrane.

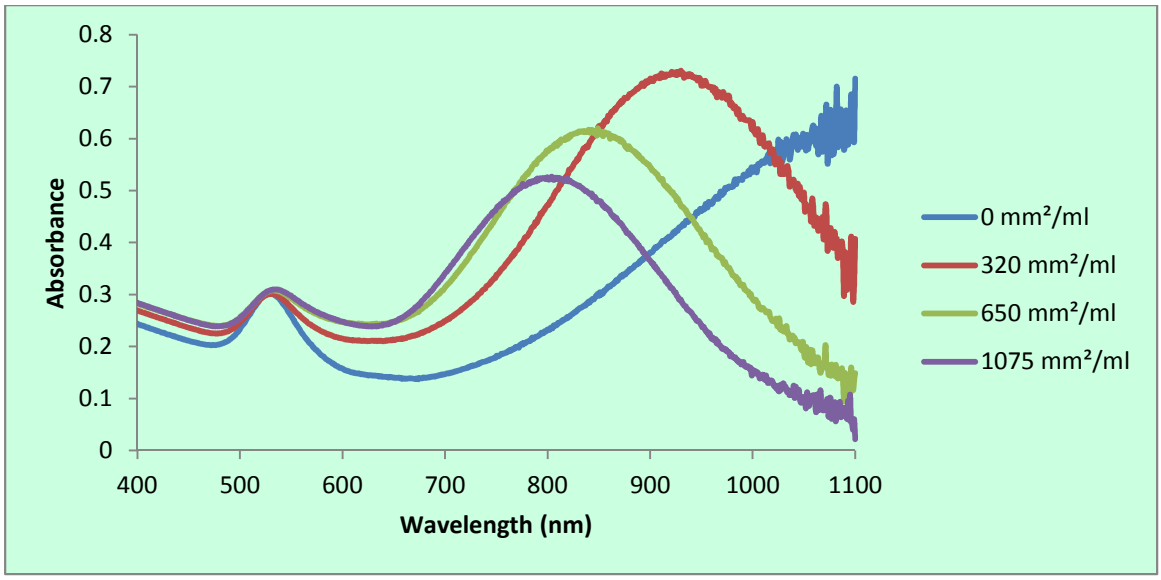

FIGURE 18 – The UV-spectra of gold/gold sulfide nanoparticles synthesized with traditional method in 50ml test tube in the presence of cellulose membrane. Varying SA/Vol ratios of cellulose to nanoparticles solution were used: 0 (blue), 320 (red), 650 (green), and 1075mm^2/ml (purple).

TABLE IV

EXPERIMENT E GGS SAMPLE PROPERTIES

	Sample	**NIR Peak**			DLS	Zeta (mV)	Temp (C)
	SA/Vol (mm2/ml)	Wavelength	Abs	OD	Size (nm)		
Avg	0	1100.00	0.73	7.30	63.42	-32.47	25.00
Std		0.00	0.03	0.26	5.20	3.36	
Avg	340	927.00	0.77	7.73	69.53	-43.37	25.00
Std		1.73	0.02	0.21	1.40	16.11	
Avg	650	843.33	0.62	6.18	66.40	-34.73	25.00
Std		7.09	0.07	0.68	3.27	2.80	
Avg	1075	803.67	0.52	5.20	65.82	-32.33	25.00
Std		5.86	0.03	0.30	1.41	5.80	

An ANOVA was performed in mintab along with a Tukey test. The SA/Vol ratio had a $P < 0.000$ and a R^2 value of 99.89%. The Tukey test shows that each of the SA/Vol picked were significantly different from one another. The residual plots are acceptable as the histogram and normal probability plot are centered around zero. The $0mm^2ml$ SPR nIR peak cannot be accurately measured, each run was assigned an estimated 1100 nm giving no calculated variance. This data proves that the hypothesis of increasing SA/Vol ratio of cellulose membrane to nanoparticles causes a blueshift of the SPR peak is correct.

F. Experiment F

This experiment proves that dialysis of ions and/or gold nanoparticles does not affect the SPR nIR peak as much as previously thought. The interaction between reactants and cellulose membrane is what drives the equilibrium shift of the SPR nIR peak. The SA/Vol still has significant effect on the equilibrium shift of the SPR absorption peak as seen in Fig. 19. The reduction of colloidal gold concentration is shown from the decrease at the 530nm absorption peak as compared to the tradition synthesis from the cellulose membrane retaining the gold nanoparticles. This alters the concentration of gold ions present during the reaction which causes a shift in SPR nIR peak. This experiment backup the hypothesis that increases in the SA/Vol ratio of cellulose to nanoparticle causes a blueshift on the SPR nIR peak. This dry Diasynth ($360mm^2/ml$) method is comparable to Experiment B's Diasynth ($240mm^2/ml$), as they have close SPR nIR peaks, but different SA/Vol ratios meaning that the exchange of ions does effect the peak as well (Fig. 20). Table V summarizes the results.

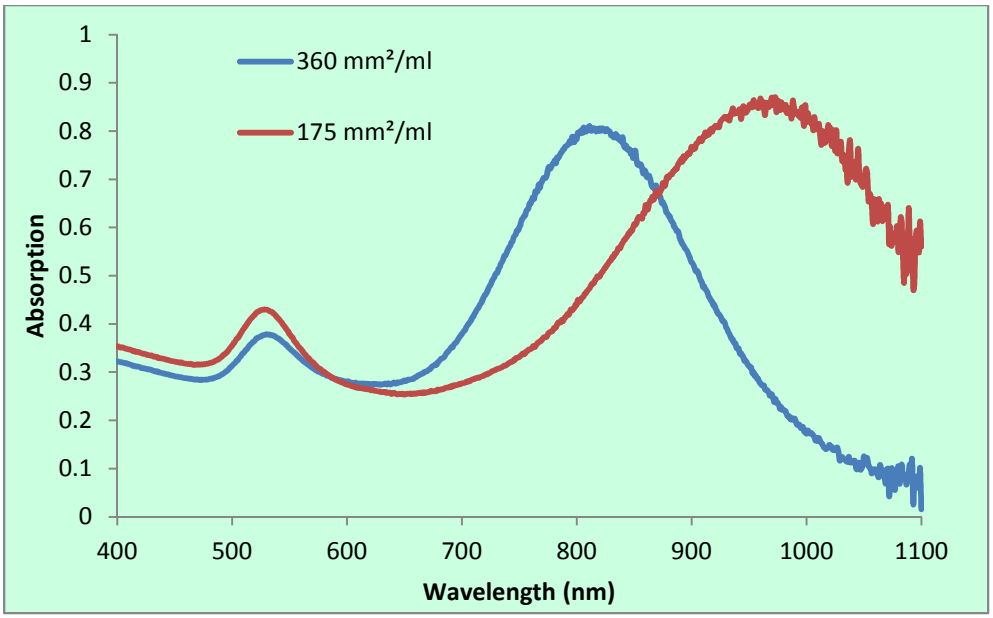

FIGURE 19 – The UV-spectra of gold/gold sulfide nanoparticles synthesized with dry Diasynth at 360mm^2/ml (blue) and 175mm^2/ml (red) SA/Vol ratios of cellulose to GGS solution with a total volume of 216ml.

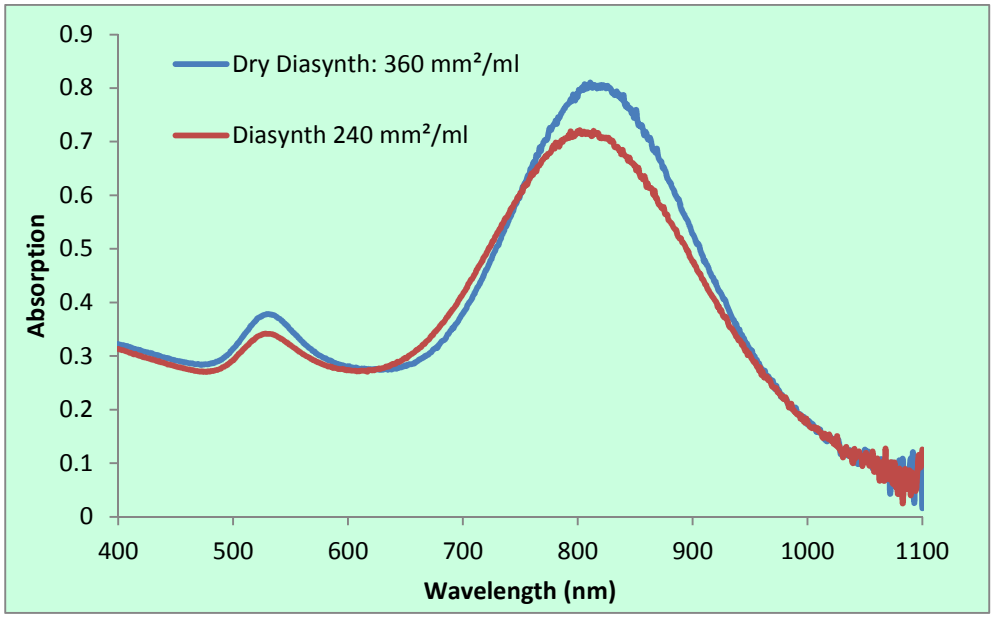

FIGURE 20 – The UV-spectra of gold/gold sulfide nanoparticles synthesized with dry Diasynth (blue) vs. Diasynth (red) method from Experiment B with a total volume of 216ml. Measured with a SA/Vol ratio of 360mm^2/ml (blue curve) and 240mm^2/ml (red curve).

TABLE V

EXPERIMENT F GGS SAMPLE PROPERTIES

Method	SA/Vol (mm^2/ml)	nIR Peak (nm)	Optical Density	Size (nm)	Zeta Potential (mV)
Dry Diasynth	175	970	8.4	54.97	-38.7
Dry Diasynth	360	817	8.0	62.47	-38.40
Diasynth	240	810	7.1	63.21	-29.9

G. Experiment G

This experiment gives information about the SA/Vol ratio of cellulose membrane to GGS nanoparticle solution and temperature effects on the SPR peak. There is a relationship with temperature and the SPR peak equilibrium shift shown in Fig. 21. The ANOVA data in Appendix I show that SA/Vol ratio, temperature, and the interaction between the two all have a significant effect on the SPR absorption peak with an R^2 value of 98.03%. The Tukey test showed that 340 and 470mm^2/ml were not significantly different from each other for temperatures at 25 and 37^oC. This data proves the hypothesis that the increase in SA/Vol of cellulose membrane to nanoparticles creates a blueshift for the SPR nIR peak. The 1st corollary was also proved here, showing that an increase in temperature causes a blueshift for the SPR nIR peak.

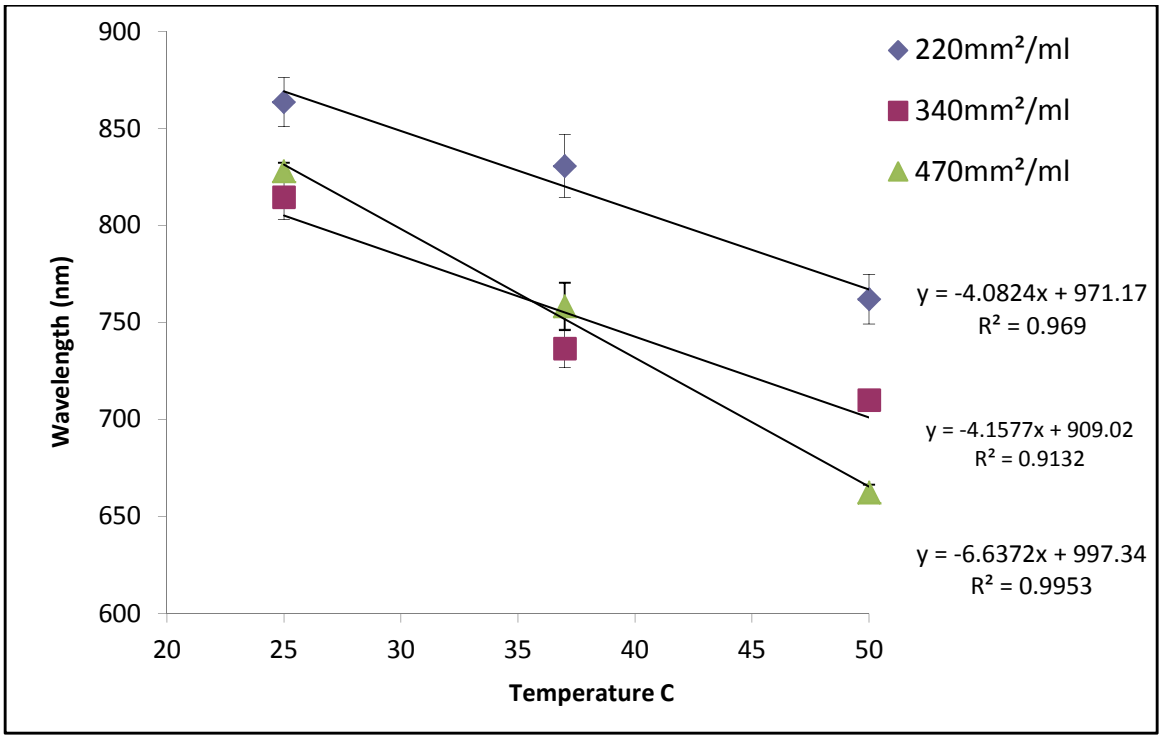

FIGURE 21 – Temperature vs. SPR nIR peak placement for 220, 340, and 470mm^2/ml. n=3

To determine the time it takes for the reaction to reach equilibrium, every 10 minutes a sample's UV-spectrum absorption was measured to determine its SPR peak placement and the time that it takes to reach equilibrium. Fig. 22 shows an example of the UV spectra of a 220mm^2/ml at 37^{o}C sample over time. Fig. 23 displays the time at which the equilibrium point is reached (20 min). Fig 24 proves the 2nd and 3rd collieries that an increase in SA/Vol ratio and/or temperature reduces the equilibrium shift time of the reaction, respectively.

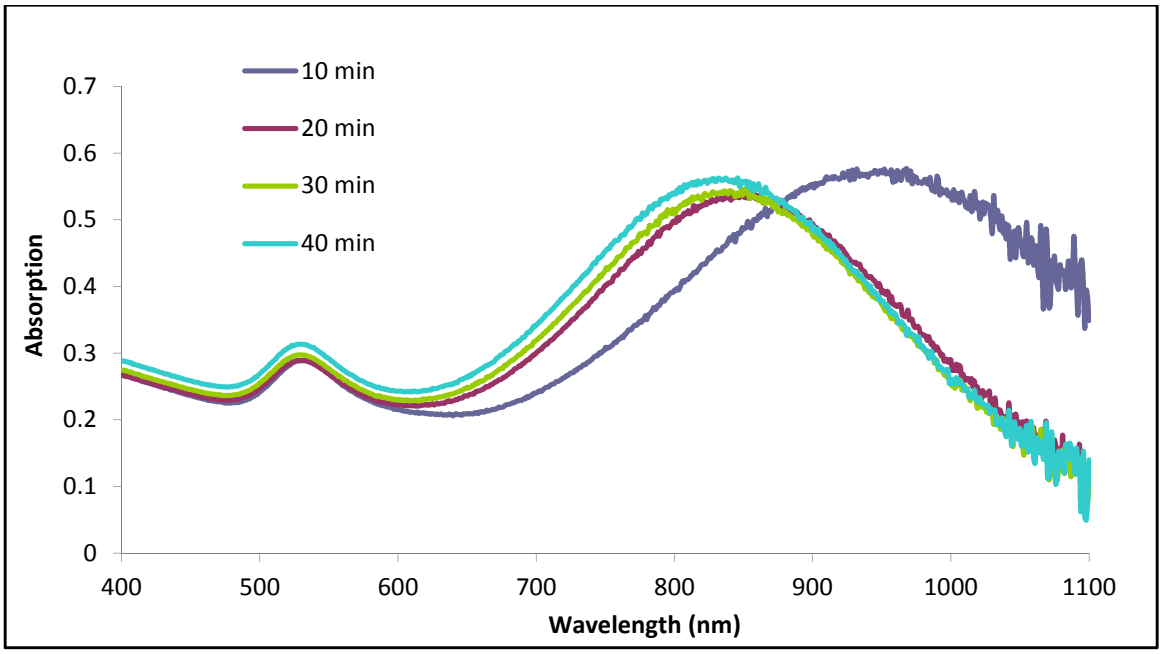

FIGURE 22 – An example showing the equilibrium shift during a Diasynth reaction

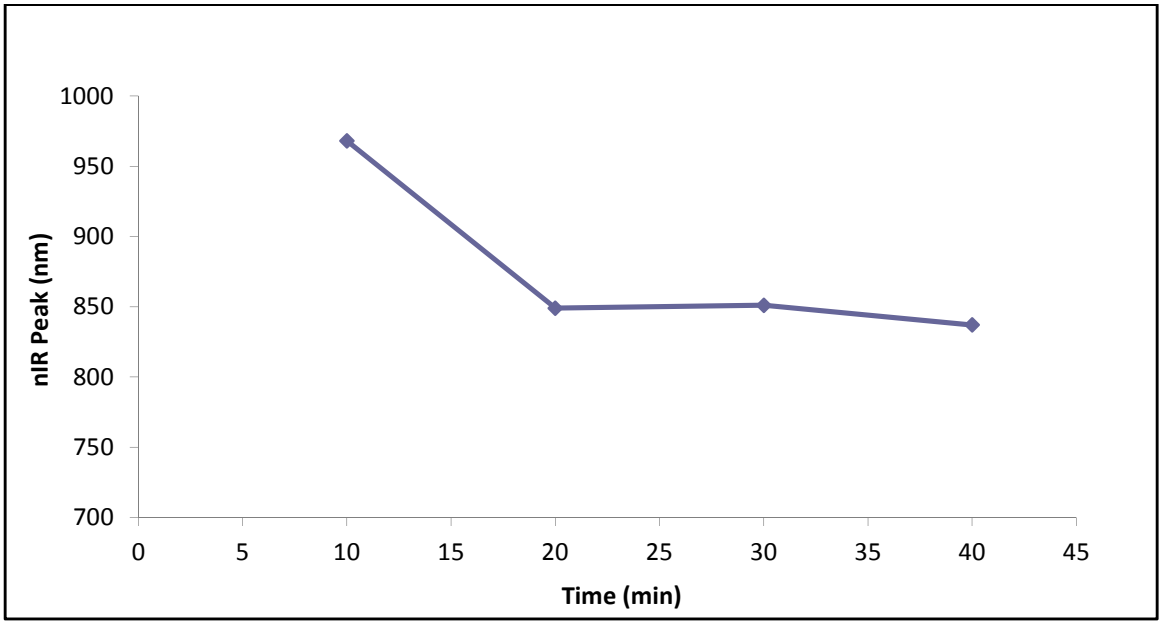

FIGURE 23 – An example showing the equilibrium point for a Diasynth sample

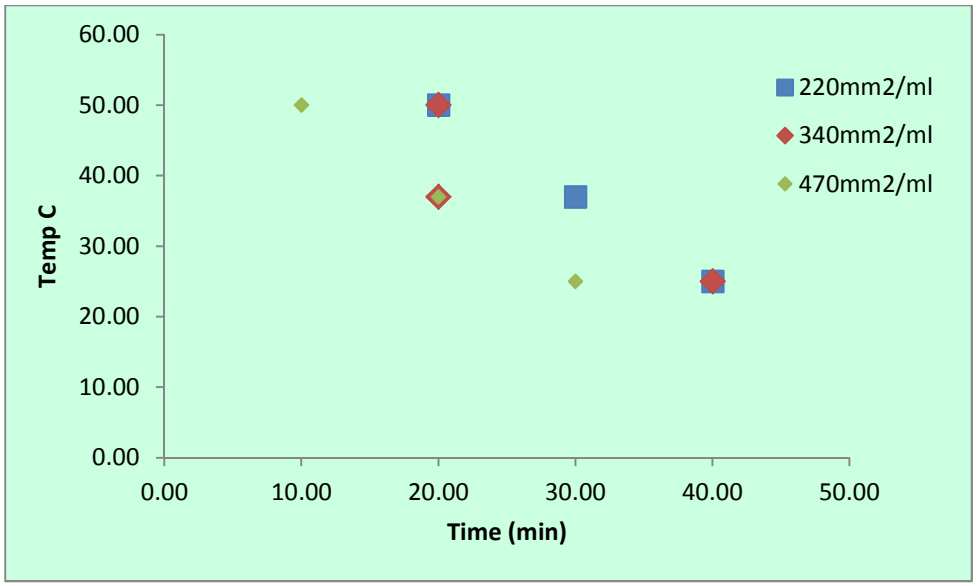

FIGURE 24 – The time (min) of that it takes to reach equilibrium vs Temperature (^{o}C) for 220, 340, and 470 mm^{2}/ml.

All of the samples' UV absorption spectra were measured at Day 0 and 14 (Fig. 25). The samples subjected to the Diasynth process seem to remain stable without being capped or protected. This proves the 4th corollary with Experiment H's stability results showing that an exchange of ions in this experiment improves stability over time wheras Experiment H has no ion exchange reducing the stability over time. The sample at 50^{o}C with a 470mm^{2}/ml was the only sample that was unstable over 14 days and is most likely due to the large SA/Vol ratio at the highest temperature point causes a fast reaction that was seen under 5 min This reaction may be too fast for stable particle formation.

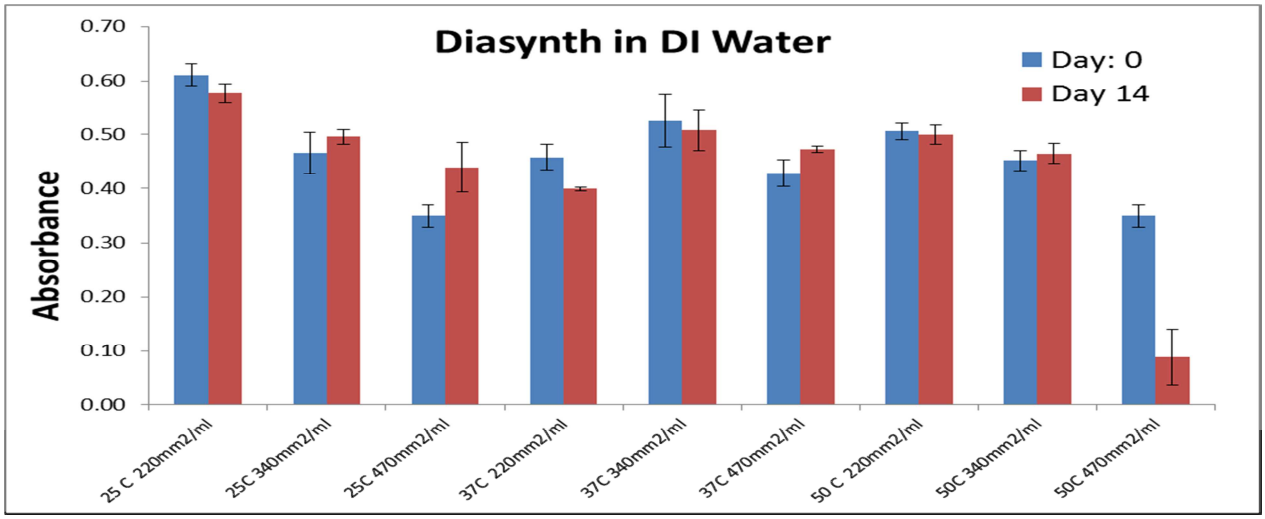

FIGURE 25 – Stability of the GGS nanoparticles after 14 days

H. Experiment H

This experiment shows the SA/Vol ratio of cellulose membrane to GGS nanoparticle solution and temperature effects on the SPR peak for dry Diasynth (no DI water). There is not a linear relationship with temperature and the SPR peak equilibrium shifts like in Experiment G shown in Fig. 26. This non-linearity is most likely from the evaporation of water from the GGS solution which causes the GGS sample to concentrate while reacting. The ANOVA data in Appendix I shows that SA/Vol ratio, temperature, and the interaction between the two all have a significant effect on the SPR absorption peak with an R^2 value of 97.53%. Similar to Experiment G, this experiment backups the hypothesis and 1st corollary that an increase in SA/Vol ratio of cellulose membrane to nanoparticles and increase in temperature has a blueshift on the SPR nIR peak, respectively.

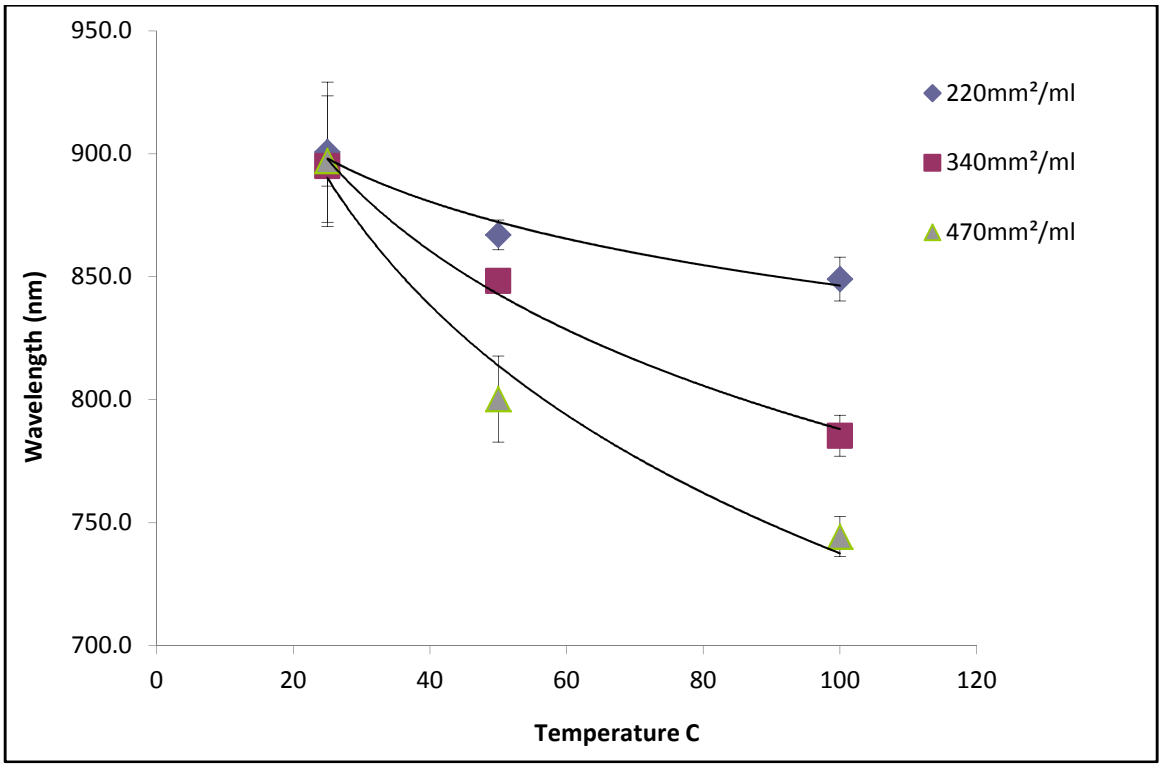

FIGURE 26 - Temperature vs. SPR nIR peak placement for 220, 340, and 470mm^2/ml for dry Diasynth. n=3

To determine the time it takes for the reaction to reach equilibrium, a sample was taken every 10 minutes to determine its SPR peak placement and the time that it takes to reach equilibrium. Fig. 22 from Experiment G shows an example of the UV spectra of a 220mm^2/ml at 37^{o}C sample over time. Fig. 23 displays the time at which the equilibrium point is reached (20 min). Fig 27 shows that an increase in SA/Vol ratio and/or temperature reduces the equilibrium shift time. The temperature most likely increases the number of collisions during the reaction, whereas it is unclear why SA/Vol reduces reaction time. Again, similar to Experiment G, the results proved the 2nd and 3rd corollaries where an increase in SA/Vol and temperature will decrease the reaction time,

respectively. 220 and 340mm^2/ml seem to have the same the same reaction time to reach equilibrium, however measurements at smaller time intervals would be needed to verify.

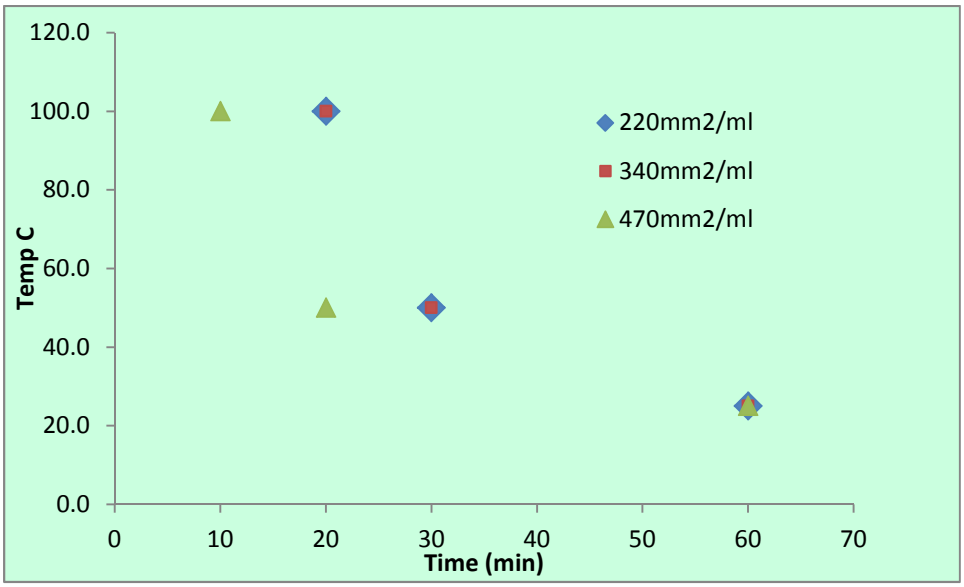

FIGURE 27 - Time (min) of equilibrium vs Temperature (^{o}C) for 220, 340, and 470 mm^2/ml.

All of the samples' UV absorption spectra was measured at Day 0 and 14. The samples that were subjected to the dry Diasynth process become unstable and aggregate over 14 days. Fig. 28 also shows the stability of the particles. This experiment confirms the 4th corollary with the stability results from Experiment G, where this experiment has no exchange of ions out of the GGS solution. The GGS nanoparticles remain stable in solution by not coming into contact with one another from the repulsion forces due to their negative surface charge. Ions can mask the surface charge of the GGS nanoparticles allowing for the repulsion forces become reduced and come into contact with other nanoparticles reacting with one another forming larger aggregates. This continues until the entire solution has aggregated.

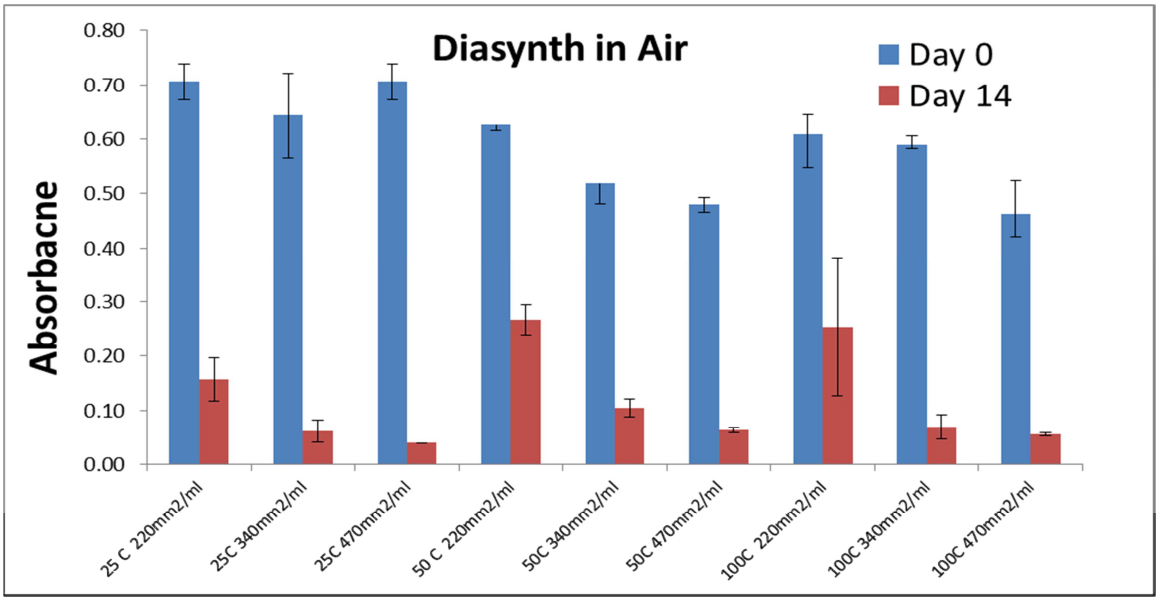

FIGURE 28 – Stability of the GGS nanoparticles after 14 days

I. Experiment I

Two different GGS samples were imaged using STEM with the Zeiss SUPRA FE-SEM. The two samples imaged have a nIR absorption peak close to 800 and 900 nm shown in Fig. 29. Image j software was used manually count and measure the size distribution data as shown in Fig. 30.

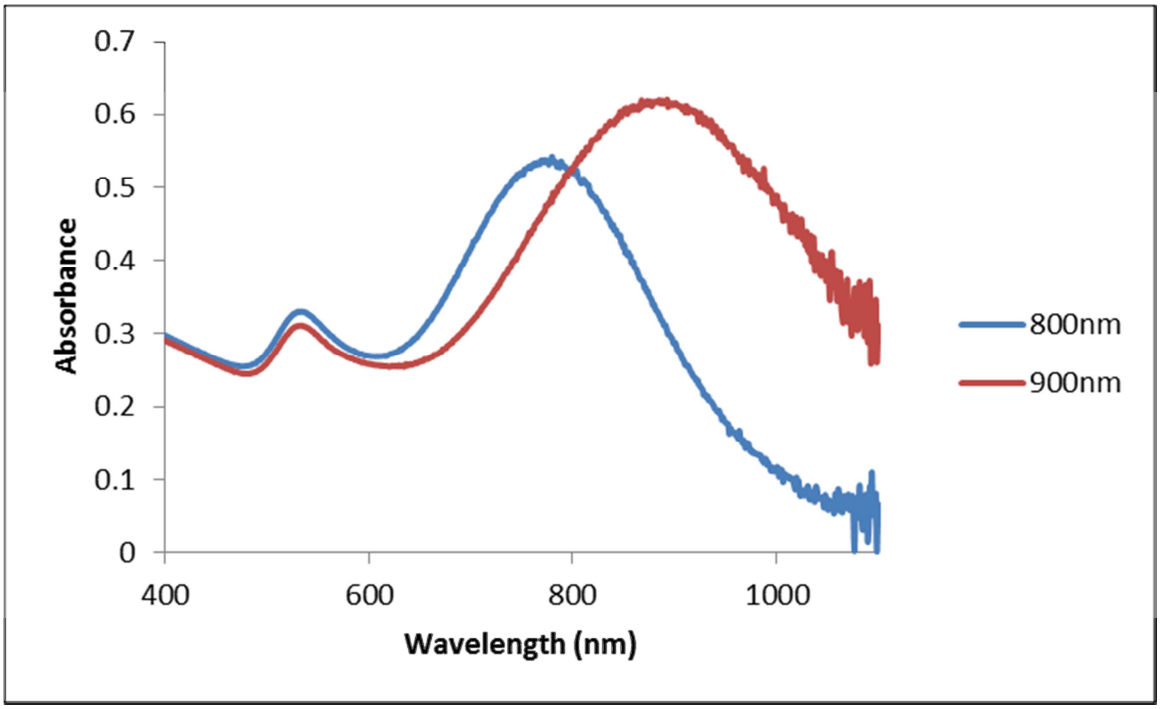

FIGURE 29 - The UV-spectra of gold/gold sulfide nanoparticles synthesized close to 800nm (blue) and 900nm (red).

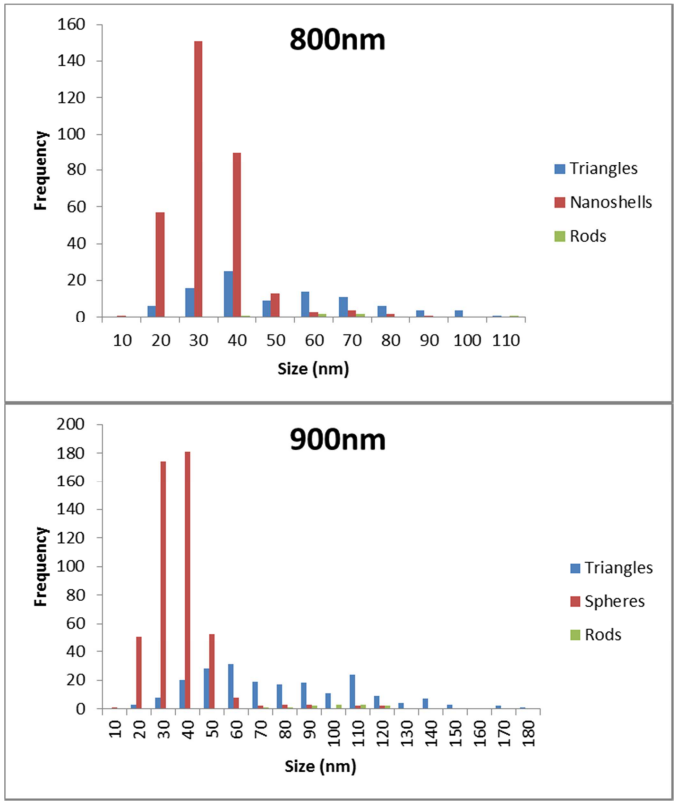

FIGURE 30 – Histogram of size distribution for two samples

TABLE VI

GGS SIZE DISTRUBUTION DATA

800nm

N=426		Count	%	AVG Size (nm)
	Shells	323	75.8	28.0
	Triangles	96	22.5	47.0
	Rods	7	1.6	69.0

900nm

N=697		Count	%	AVG Size
	Shells	480	68.9	32.0
	Triangles	205	29.4	72.8
	Rods	12	1.7	94.1

The average size in Table VI refers to diameter, edge length, and length for nanoshells, nanotriangles, and nanorods respectively. The images used for the histogram were Figs. 38-40 for 800 and Figs. 41-43 for 900nm in Appendix III. The edge length of the nanotriangles increase in size from the 800 to 900 nm sample, which follows the same trend with findings by Young et al. (Young et al., 2012). The nanoshells also increase in size from the 800nm sample to the 900nm sample. Mie theory needs to be performed to determine the core and shell dimensions.

IV. CONCLUSION

It was demonstrated in this paper that ions are diffusing out of the cellulose membrane during the Diasynth process. These ions do not have a significant effect on the equilibrium shift of the surface plasmon absorption as previously thought. However,

these ions do affect the stability of non-coated GGS nanoparticles. The GGS particles that dialyzed out of the ions remained stable for up to 2 weeks whereas the particles which had no dialysis aggregated. It was discovered that the cellulose membrane retains the small gold colloid (<10 nm) that was problematic before with the traditional synthesis that required purification.

The Diasynth method has shown to be able to increase in synthesis volume from 50ml (Patel, 2012) to 216ml. Not shown in this paper, but the volume has been scaled up even further to 500ml with control over SPR peak placement. Further volume increase can be performed with more precise control over the reaction by adjusting molar ratio, temperature, and/or surface area to volume ratio of cellulose membrane to gold/gold-sulfide nanoparticles. The SA/Vol ratio and temperature were found to significantly affect the SPR equilibrium shift. The temperature SA/Vol ratio not only helps to control the surface plasmon resonance peak, but also reduce the time the reaction takes.

V. RECOMMENDATIONS

There is still room for potential expansion upon this synthesis process. Using Na_2S with the Diasynth method (wet or dry) could give better stable GGS nanoparticles. From Eq. 1, there are fewer ions associated with this reaction which could yield a more stable GGS solution as well as be performed with the dry Diasynth method. Mie theory calculations can be performed to determine the nanoshell thickness from Experiment I's data. Better initial mixing techniques of the two reactants should be investigated, as this now will begin to affect the volumetric scale up process due to initial colloidal gold

formation. The largest reaction thus far has been 500 ml which had an nIR peak at 820 nm. An important future work would be to increase the volume of the reaction to 1 L.

APPENDIX I

Experiment E

Minitab
General Linear Model: Wavelength versus SA/Vol

```
Factor  Type   Levels  Values
SA/Vol  fixed       4  0.0, 320.0, 650.0, 1075.0


Analysis of Variance for Wavelength, using Adjusted SS for Tests

Source  DF  Seq SS  Adj SS  Adj MS        F      P
SA/Vol   3  155554  155554   51851  2365.84  0.000
Error    8     175     175      22
Total   11  155729


S = 4.68152   R-Sq = 99.89%   R-Sq(adj) = 99.85%


Unusual Observations for Wavelength

Obs  Wavelength     Fit  SE Fit  Residual  St Resid
  8      851.00  843.33    2.70      7.67      2.01 R

R denotes an observation with a large standardized residual.


Grouping Information Using Tukey Method and 95.0% Confidence

SA/Vol  N    Mean  Grouping
   0.0  3  1100.0  A
 320.0  3   927.0     B
 650.0  3   843.3       C
1075.0  3   803.7         D

Means that do not share a letter are significantly different.
```

Residual Plots for Wavelength

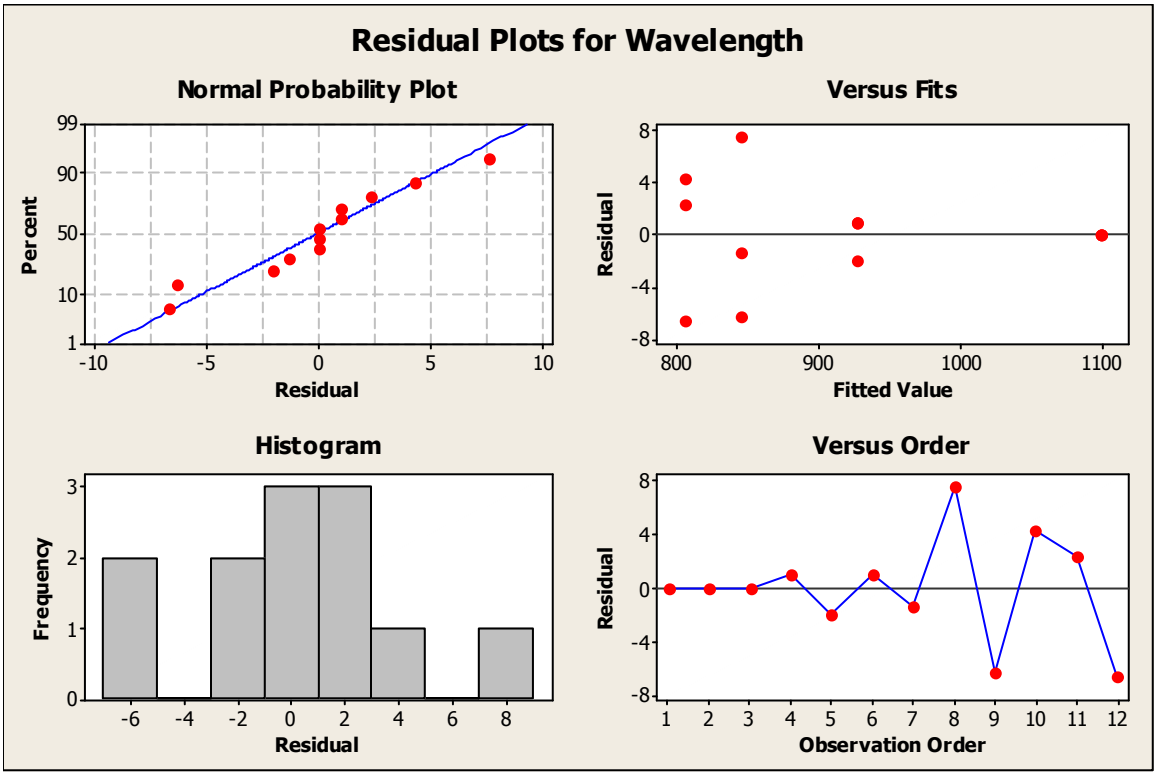

FIGURE 31 – Residual Plots for Experiment E

MINITAB
General Linear Model: wavelength versus Temp (C), SA (mm2/ml)

```
Factor       Type   Levels  Values
Temp (C)     fixed       3  25, 37, 50
SA (mm2/ml)  fixed       3  220, 340, 470


Analysis of Variance for wavelength, using Adjusted SS for Tests

Source                 DF  Seq SS  Adj SS  Adj MS       F      P
Temp (C)                2   69207   69207   34603  302.75  0.000
SA (mm2/ml)             2   27082   27082   13541  118.47  0.000
Temp (C)*SA (mm2/ml)    4    6198    6198    1550   13.56  0.000
Error                  18    2057    2057     114
Total                  26  104545


S = 10.6909   R-Sq = 98.03%   R-Sq(adj) = 97.16%


Unusual Observations for wavelength

Obs  wavelength      Fit  SE Fit  Residual  St Resid
  4     812.000  830.667   6.172   -18.667     -2.14 R

R denotes an observation with a large standardized residual.


Grouping Information Using Tukey Method and 95.0% Confidence

Temp
(C)   N   Mean  Grouping
25    9  835.4  A
37    9  775.2     B
50    9  711.4        C

Means that do not share a letter are significantly different.


Grouping Information Using Tukey Method and 95.0% Confidence

SA
(mm2/ml)  N   Mean  Grouping
220       9  818.8  A
340       9  753.8     B
470       9  749.6     B

Means that do not share a letter are significantly different.


Grouping Information Using Tukey Method and 95.0% Confidence

Temp  SA
(C)   (mm2/ml)  N   Mean  Grouping
25    220       3  863.6  A
37    220       3  830.7     B
```

25	470	3	828.0	B		
25	340	3	814.7	B		
50	220	3	762.0		C	
37	470	3	758.3		C	
37	340	3	736.7		C	D
50	340	3	710.0			D
50	470	3	662.3			E

Means that do not share a letter are significantly different.

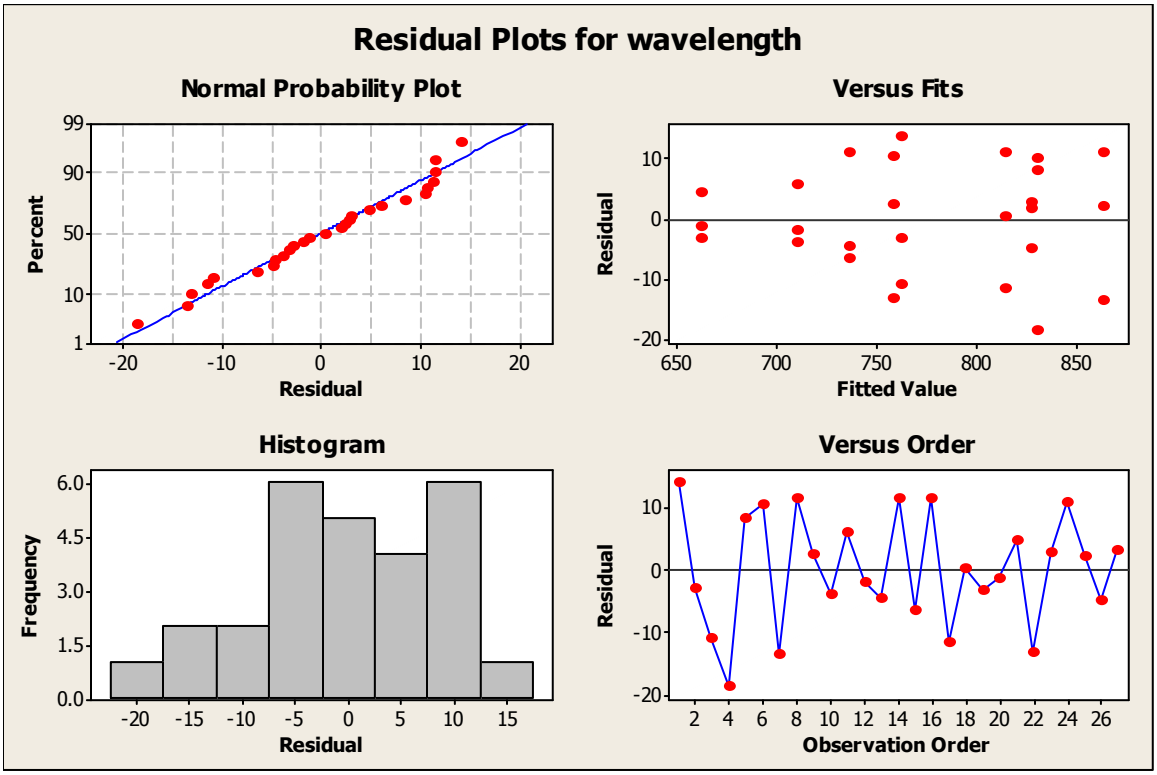

FIGURE 32 – Residual plots for Experiment G

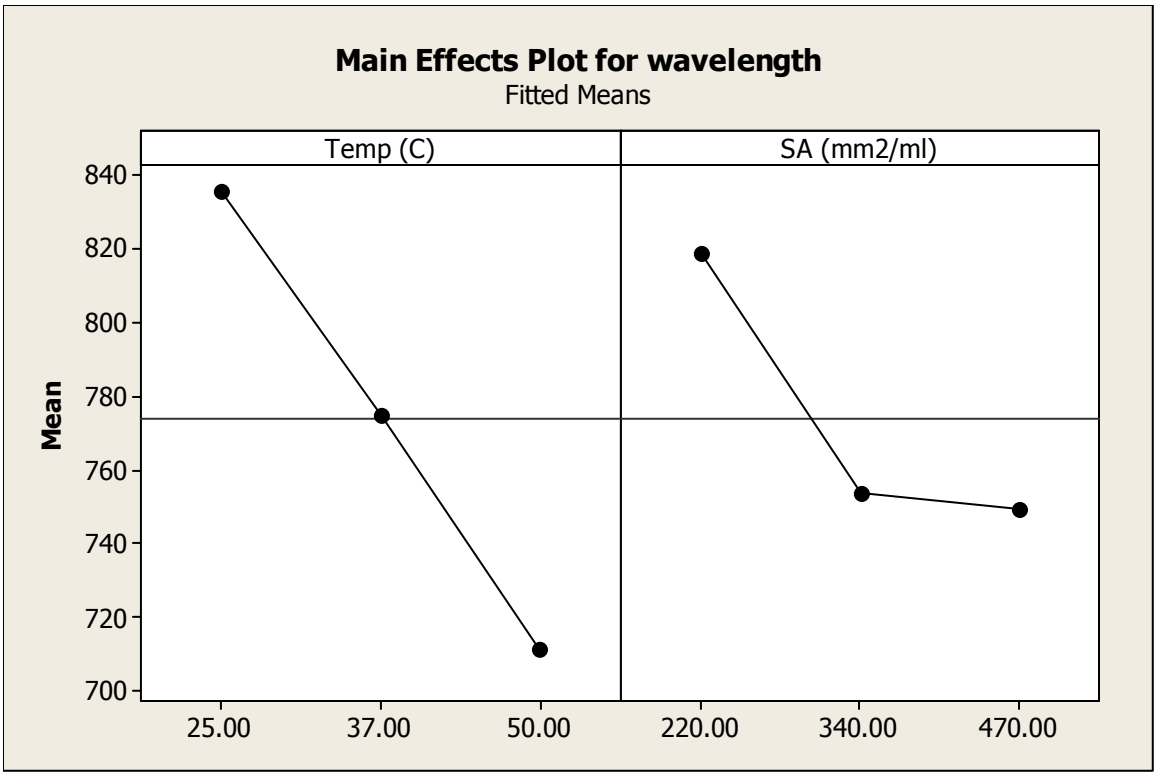

FIGURE 33 –Main Effects plots for Experiment G

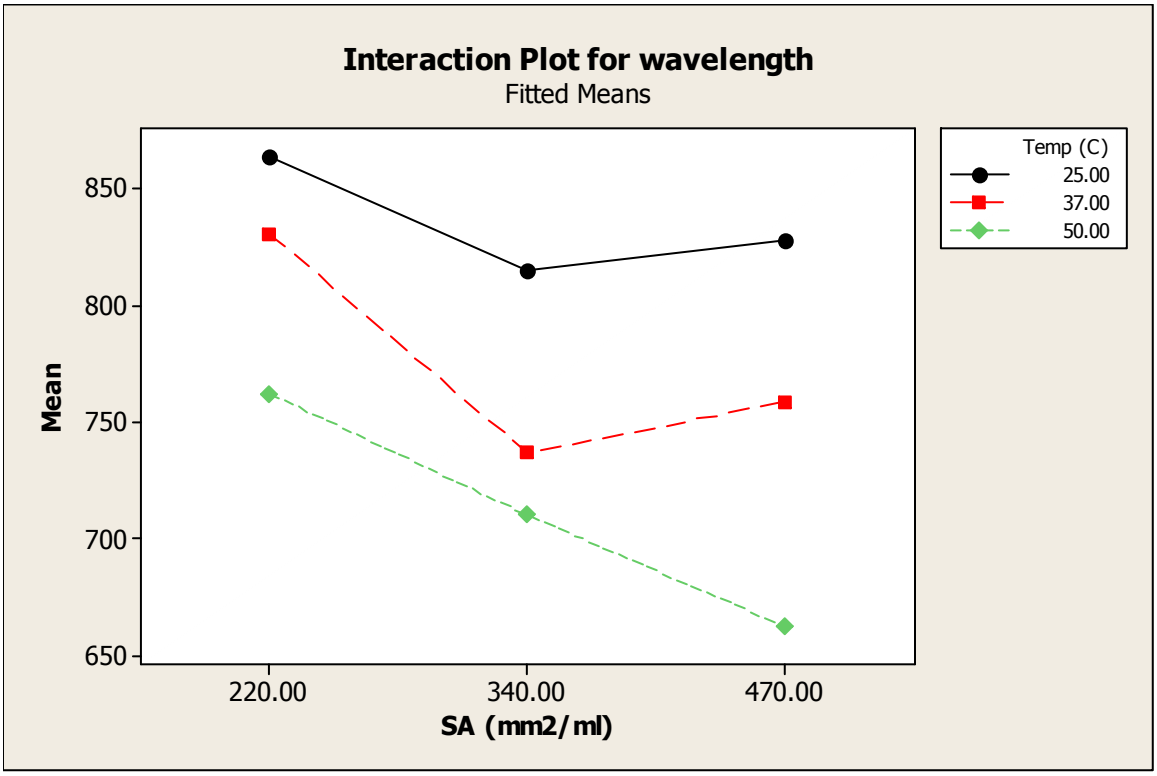

FIGURE 34 – Interaction plot for Experiment G

General Linear Model: Wavelength versus Temp, SA/Vol

```
Factor  Type   Levels  Values
Temp    fixed       3  25, 50, 100
SA/Vol  fixed       3  220, 340, 470


Analysis of Variance for Wavelength, using Adjusted SS for Tests

Source       DF   Seq SS   Adj SS   Adj MS       F      P
Temp          2  52220.4  52220.4  26110.2  243.67  0.000
SA/Vol        2  14689.9  14689.9   7344.9   68.55  0.000
Temp*SA/Vol   4   9129.7   9129.7   2282.4   21.30  0.000
Error        18   1928.7   1928.7    107.2
Total        26  77968.7


S = 10.3515   R-Sq = 97.53%   R-Sq(adj) = 96.43%


Unusual Observations for Wavelength

Obs  Wavelength      Fit  SE Fit  Residual  St Resid
  2     817.935  800.283   5.976    17.652      2.09 R
  3     782.961  800.283   5.976   -17.323     -2.05 R
  8     923.000  901.000   5.976    22.000      2.60 R

R denotes an observation with a large standardized residual.


Grouping Information Using Tukey Method and 95.0% Confidence

Temp  N   Mean  Grouping
 25   9  900.2  A
 50   9  838.5    B
100   9  792.9      C

Means that do not share a letter are significantly different.


Grouping Information Using Tukey Method and 95.0% Confidence

SA/Vol  N   Mean  Grouping
220     9  872.3  A
340     9  844.1    B
470     9  815.2      C

Means that do not share a letter are significantly different.


Grouping Information Using Tukey Method and 95.0% Confidence

Temp  SA/Vol  N   Mean  Grouping
 25   470     3  901.0  A
 25   220     3  901.0  A
 25   340     3  898.7  A
 50   220     3  867.0    B
100   220     3  849.0    B
 50   340     3  848.3    B
```

```
 50    470      3   800.3       C
100    340      3   785.3       C
100    470      3   744.3         D
```

Means that do not share a letter are significantly different.

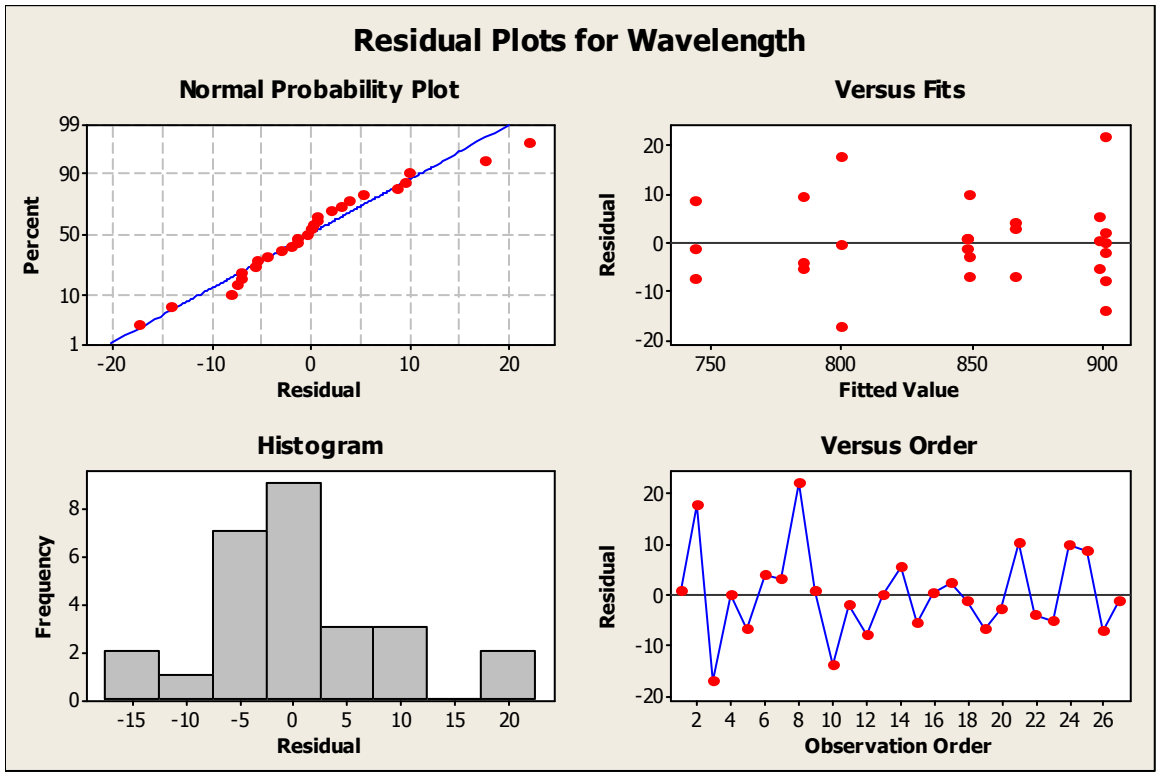

FIGURE 35 – Residual plots for Experiment H

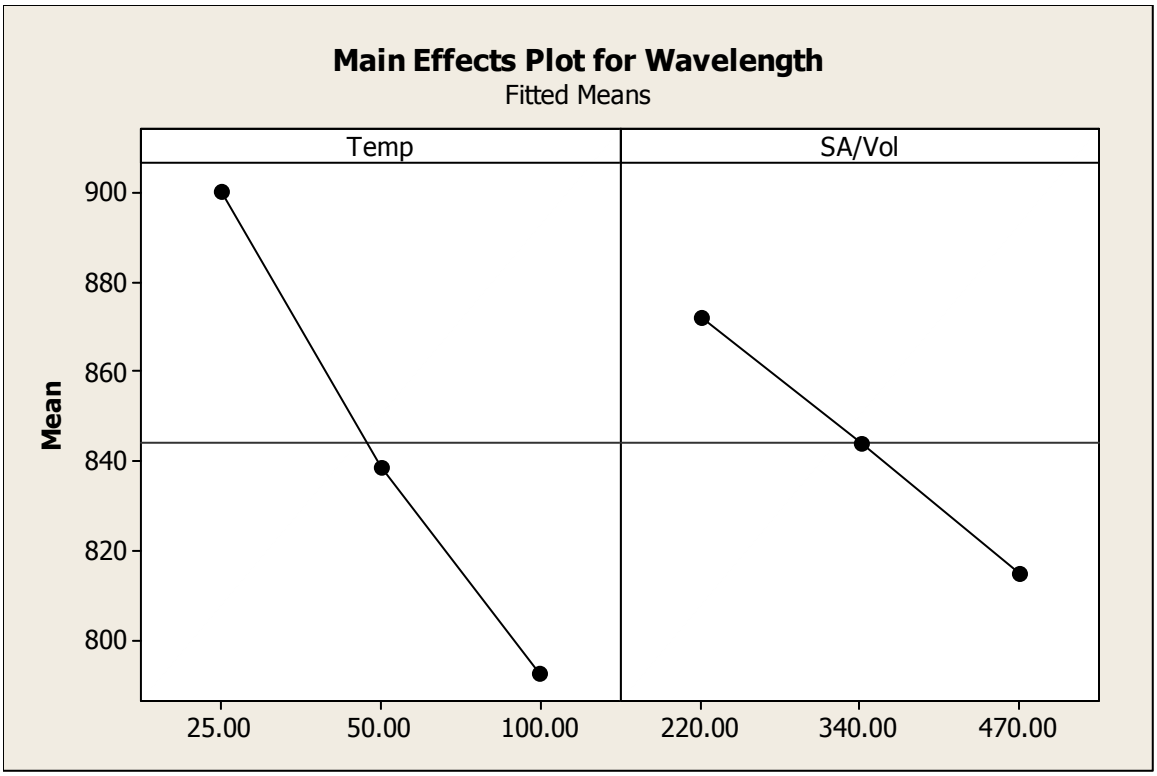

FIGURE 36 – Main effects plots for Experiment H

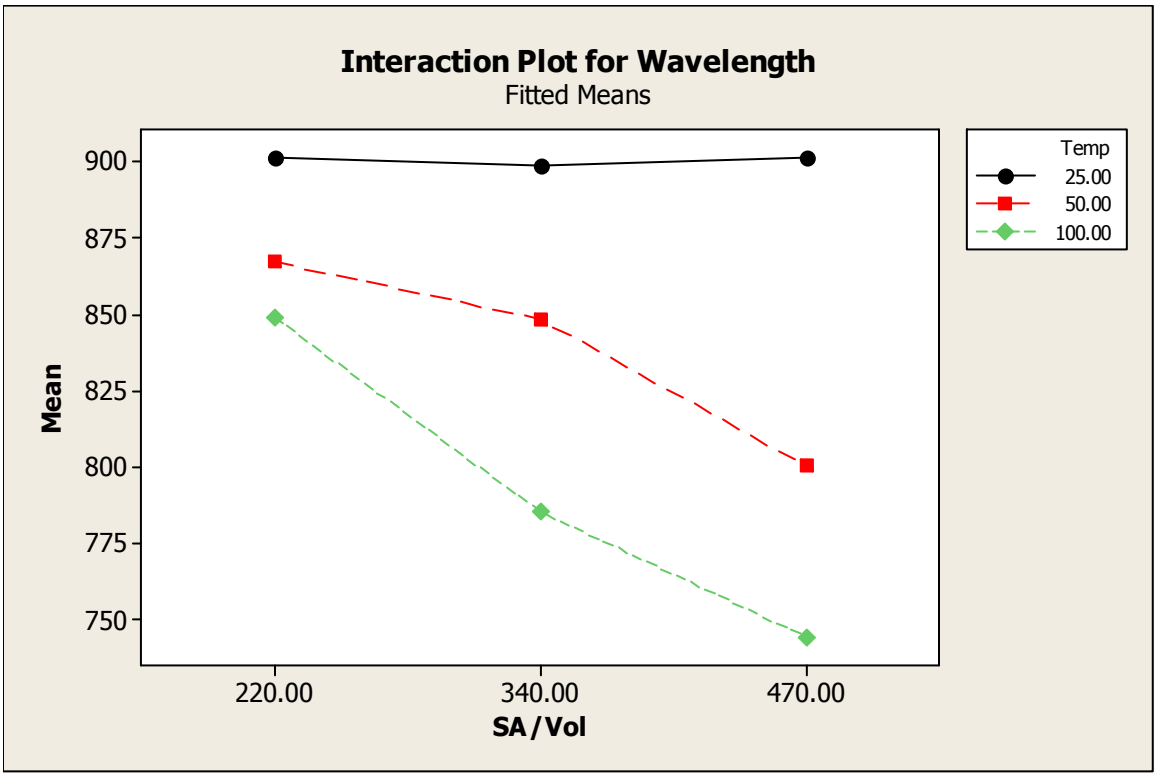

FIGURE 37 – Interaction plot for Experiment H

APPENDIX II

TABLE VII

EXPERIMENT G SAMPLE PROPERTIES

Sample	NIR Peak wavelength	OD	Ratio* NIR/Coll	Size (nm)	Temp (C)	SA (mm2/ml)	Time (min)
Diasynth 14	775.96	5.29	1.60	56.92	50.00	220.00	10.00
Diasynth15	758.95	5.00	1.55	59.24	50.00	220.00	20.00
Diasynth19	751.05	4.99	1.47	55.11	50.00	220.00	20.00
Avg	761.99	5.09	1.54	57.09	50.00	220.00	20.00
Std	12.73	0.17	0.06	2.07	0.00	0.00	
Diasynth29	812	4.702	1.61	57.01	37	220	20
Diasynth30	839	5.465	1.84	58.04	37	220	30
Diasynth31	841	5.436	1.75	59.71	37	220	20
Avg	830.7	5.201	1.732	58.3	37	220	30
Std	16.20	0.43	0.12	1.36	0.00	0.00	
Diasynth23	850	4.140	1.64	68.7	25	220	30
Diasynth24	875	4.965	1.85	74.63	25	220	30
Diasynth25	866	5.383	1.85	81.03	25	220	40
Avg	863.6	4.829	1.780	74.8	25	260	40
Std	12.66	0.63	0.12	6.17	0.00	69.28	
Sample	NIR Peak wavelength	OD	Ratio* NIR/Coll	Size (nm)	Temp (C)	SA (mm2/ml)	Time (min)
Diasynth16	706.00	4.31	1.41	49.02	50.00	340.00	10.00
Diasynth17	716.04	4.62	1.45	54.87	50.00	340.00	20.00
Diasynth18	708.01	4.63	1.39	53.69	50.00	340.00	20.00
Avg	710.02	4.52	1.42	52.53	50.00	340.00	20.00
Std	5.31	0.18	0.03	3.09	0.00	0.00	
Diasynth26	732	4.357	1.46	58.95	37	340	20
Diasynth27	748	4.357	1.47	62.75	37	340	20
Diasynth28	730	4.126	1.48	60.29	37	340	20
Avg	736.7	4.280	1.470	60.7	37	340	20
Std	9.85	0.13	0.01	1.93	0.00	0.00	0.00
Diasynth20	826.05	4.23	1.60	68.42	25.00	340.00	40.00
Diasynth21	803.01	4.51	1.69	69.02	25.00	340.00	30.00
Diasynth22	815.04	4.67	1.79	69.70	25.00	340.00	30.00
Avg	814.70	4.47	1.69	69.05	25.00	340.00	40.00
Std	11.53	0.22	0.10	0.64	0.00	0.00	

Diasynth32	659	3.265	1.11	51.52	50	470	10
Diasynth33	661	3.595	1.17	54.11	50	470	10
Diasynth34	667	3.623	1.21	53.26	50	470	10
Avg	662.3	3.494	1.162	53.0	50	470	10
Std	4.2	0.199	0.0	1.32	0.0	0.0	0.0
Diasynth35	745	4.042	1.44	59.31	37	470	20
Diasynth36	761	4.535	1.47	60.83	37	470	20
Diasynth37	769	4.264	1.50	62.43	37	470	20
Avg	758.3	4.280	1.468	60.9	37	470	20
Std	12.2	0.247	0.0	1.56	0.0	0.0	0.0
Diasynth38	830	4.412	1.70	69.25	25	470	30
Diasynth39	823	4.377	1.68	74.93	25	470	30
Diasynth40	831	4.479	1.67	68.37	25	470	30
Avg	828.0	4.423	1.682	70.9	25	470	30
Std	4.4	0.052	0.0	3.56	0.0	0.0	0.0

TABLE VIII

EXPERIMENT H SAMPLE PROPERTIES

Sample	**NIR Peak**		**Ratio***	Size (nm)	Temp (C)	SA (mm2/ml)	Time (min)
	wavelength	OD	NIR/Coll				
MR19	923	7.536	2.19	72	25	220	60
MR20	887	7.288	2.15	86.37	25	220	60
MR21	893	6.823	2.06	84.89	25	220	60
Avg	901.0	7.2	2.1	81.1	25.0	220.0	60.0
Std	19.29	0.36	0.06	7.90	0.00	0.00	0.00

Sample	**NIR Peak**		**Ratio***	Size (nm)	Temp (C)	SA (mm2/ml)	Time (min)
	wavelength	OD	NIR/Coll				
MR22	904	5.884	1.94	76.3	25	340	60
MR23	893	6.207	2.00	78.43	25	340	60
MR24	899	6.988	2.00	76.33	25	340	60
Avg	898.7	6.359	1.982	77.0	25	340	60
Std	5.49	0.57	0.03	1.22	0.00	0.00	34.64

Sample	**NIR Peak**	**Ratio***	Size (nm)	Temp (C)	SA (mm2/ml)	Time (min)

	wavelength	OD	NIR/Coll				
MR25	903	5.282	2.00	82.27	25	470	60
MR20	899	7.288	2.15	86.37	25	470	60
MR21	901	6.823	2.06	84.89	25	470	60
Avg	901.0	6.5	2.1	84.5	25.0	470.0	60.0
Std	2.00	1.05	0.08	2.08	0.00	0.00	0.00

Sample	NIR Peak		Ratio*	Size (nm)	Temp (C)	SA (mm2/ml)	Time (min)
	wavelength	OD	NIR/Coll				
MR16	860.00	6.19	2.07	87.70	50	220	30
MR17	870.93	6.18	2.12	73.20	50	220	30
MR18	869.99	6.35	1.97	94.20	50	220	30
Avg	866.97	6.24	2.05	85.03	50	220	30
Std	6.06	0.09	0.08	10.75			

Sample	NIR Peak		Ratio*	Size (nm)	Temp (C)	SA (mm2/ml)	Time (min)
	wavelength	OD	NIR/Coll				
MR1	849.01	4.92	1.73	104.60	50.00	340.00	30.00
MR2	849.01	4.55	1.76	74.65	50.00	340.00	30.00
MR3	846.97	5.43	1.74	76.76	50.00	340.00	30.00
Avg	848.33	4.97	1.74	85.34	50.00	340.00	30.00
Std	1.18	0.45	0.01	16.72	0.00	0.00	0.00

Sample	NIR Peak		Ratio*	Size (nm)	Temp (C)	SA (mm2/ml)	Time (min)
	wavelength	OD	NIR/Coll				
MR13	817.94	4.91	1.56	76.63	50.00	470.00	20.00
MR14	782.96	4.49	1.48	76.85	50.00	470.00	20.00
MR15	799.95	4.70	1.54	64.72	50.00	470.00	20.00
Avg	800.28	4.70	1.53	72.73	50.00	470.00	20.00
Std	17.49	0.21	0.04	6.94	0.00	0.00	0.00

Sample	NIR Peak		Ratio*	Size (nm)	Temp (C)	SA (mm2/ml)	Time (min)
	wavelength	OD	NIR/Coll				
MR4	842.07	5.67	1.82	68.03	100.00	220.00	20.00
MR5	846.02	5.17	1.78	67.54	100.00	220.00	20.00
MR6	859.05	6.52	1.86	68.33	100.00	220.00	20.00
Avg	849.05	5.78	1.82	67.97	100.00	220.00	20.00
Std	8.89	0.68	0.04	0.40	0.00	0.00	0.00

Sample	NIR Peak		Ratio*	Size (nm)	Temp (C)	SA (mm2/ml)	Time (min)
	wavelength	OD	NIR/Coll				
MR10	781.00	5.96	1.63	67.03	100.00	340.00	20.00
MR11	780.02	5.43	1.64	69.20	100.00	340.00	20.00
MR12	794.95	5.85	1.62	61.94	100.00	340.00	20.00
Avg	785.33	5.75	1.63	66.06	100.00	340.00	20.00
Std	8.35	0.28	0.01	3.73	0.00	0.00	0.00

Sample	NIR Peak		Ratio*	Size (nm)	Temp (C)	SA (mm2/ml)	Time (min)
	wavelength	OD	NIR/Coll				
MR7	753.02	4.93	1.53	63.93	100.00	470.00	10.00
MR8	737.01	4.47	1.45	64.07	100.00	470.00	10.00
MR9	742.97	4.33	1.43	61.35	100.00	470.00	10.00
Avg	744.34	4.57	1.47	63.12	100.00	470.00	10.00
Std	8.09	0.31	0.05	1.53	0.00	0.00	0.00

APPENDIX III

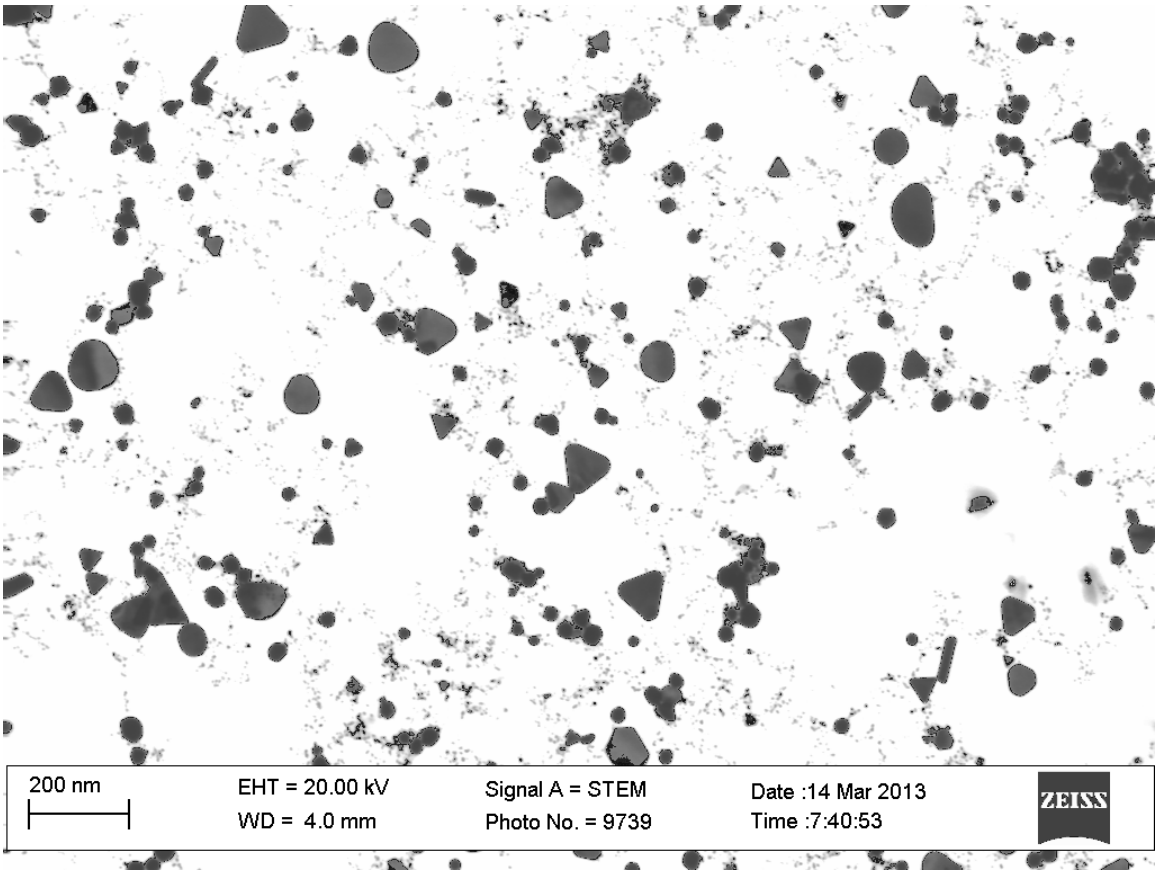

FIGURE 38 - STEM Image 01

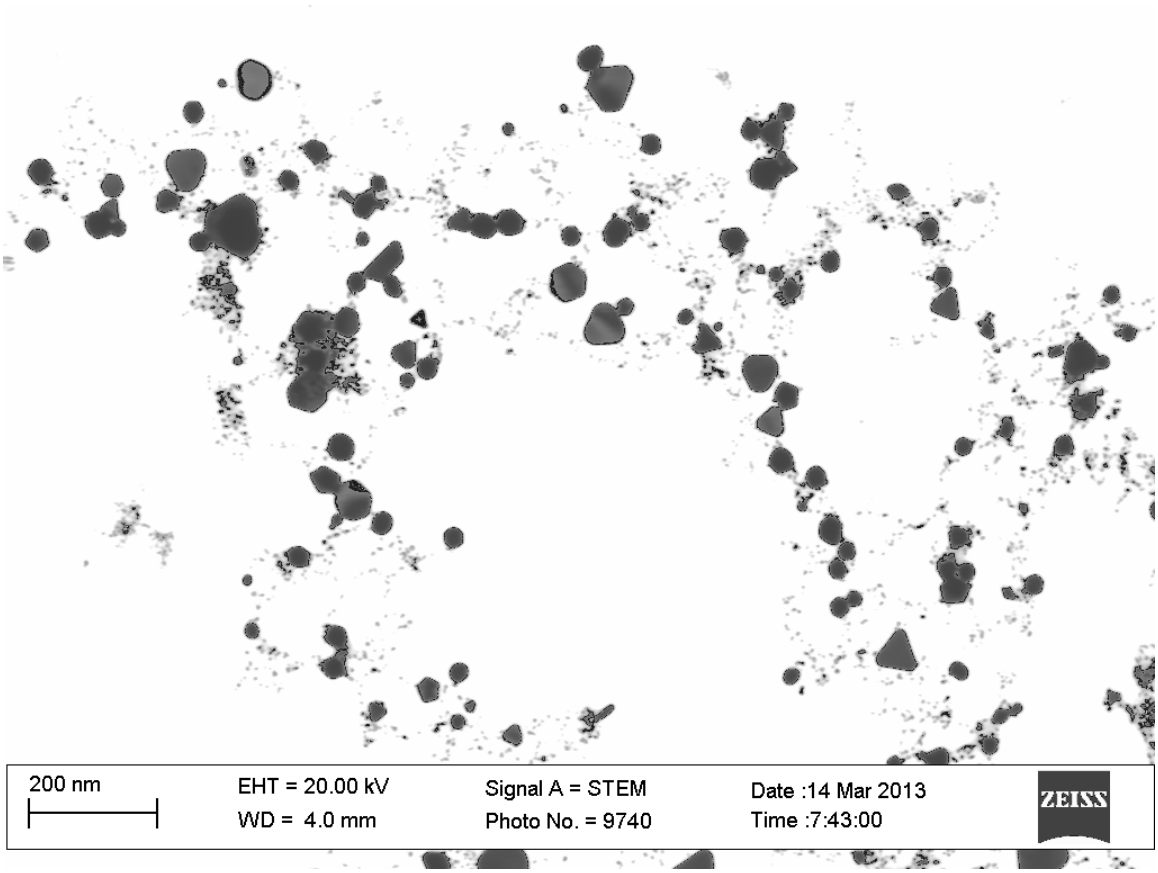

FIGURE 39 - STEM Image 02

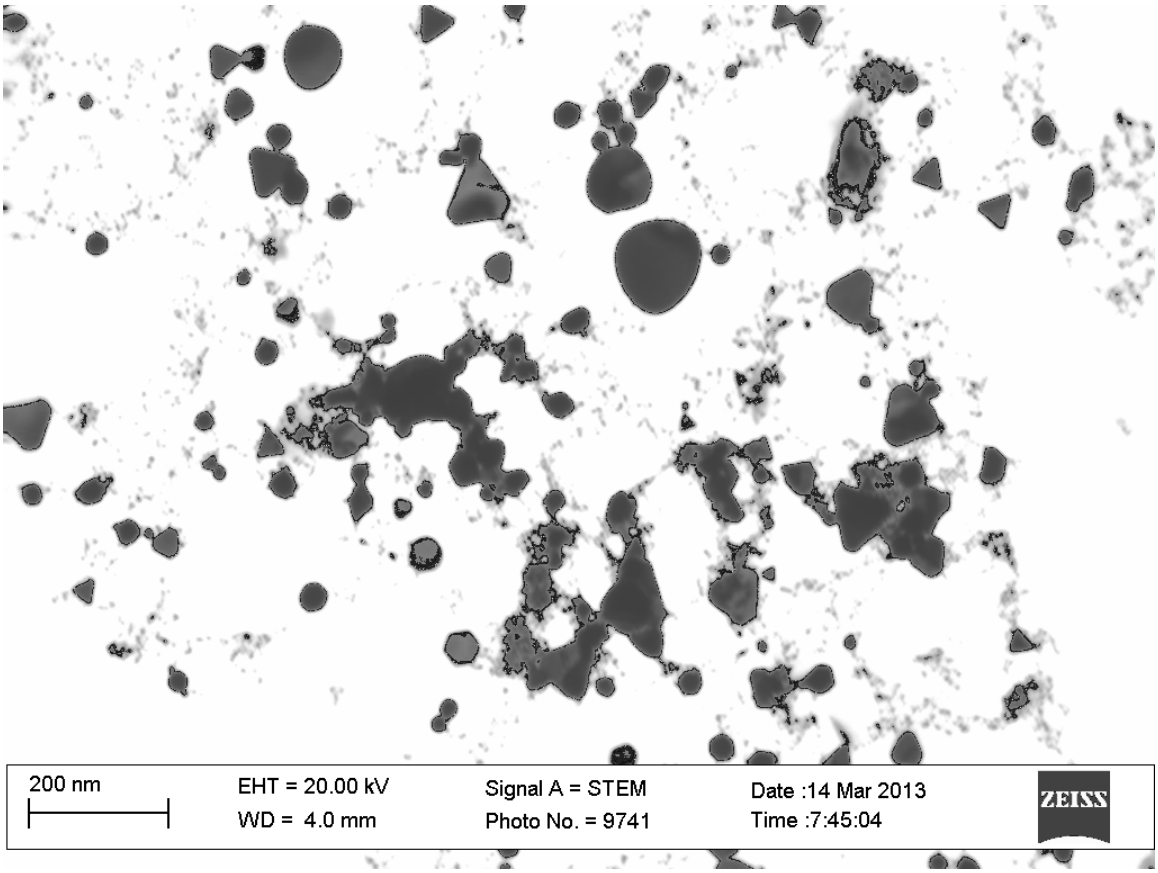

FIGURE 40 - STEM Image 03

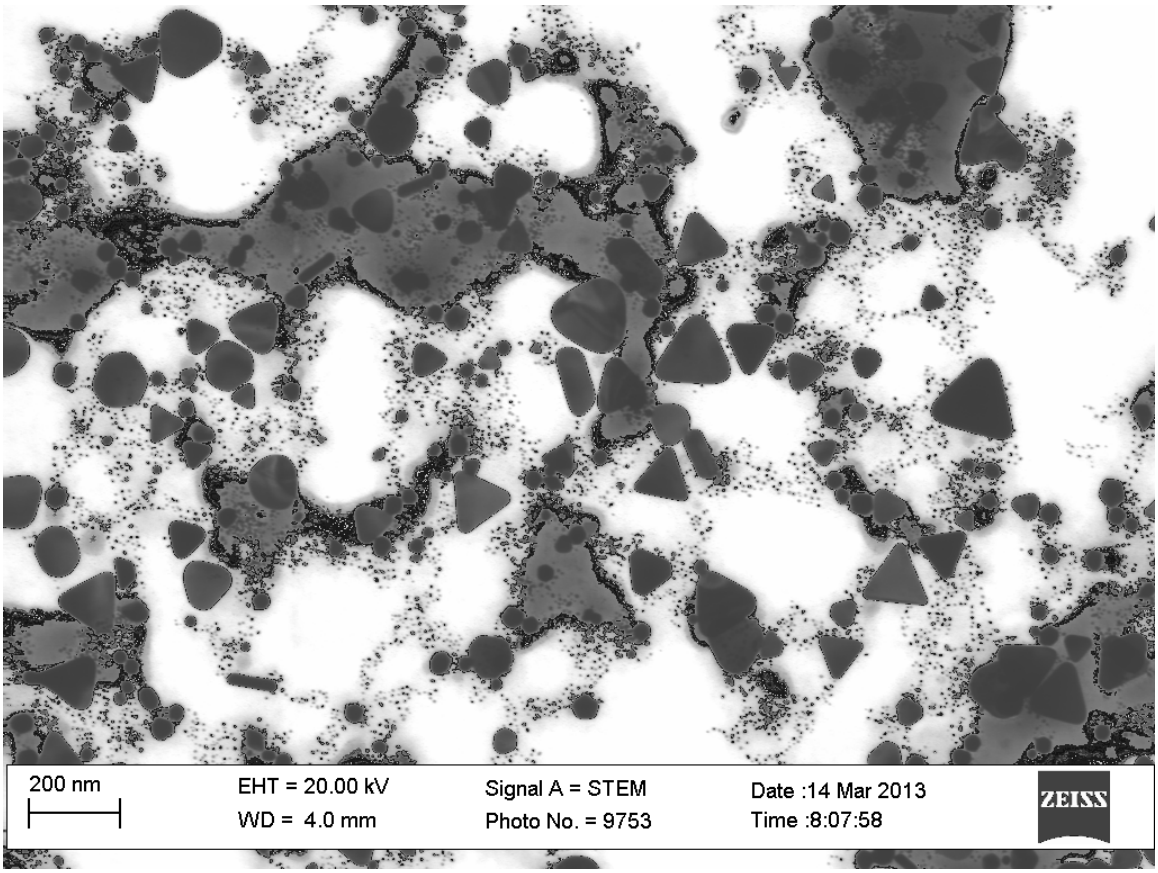

FIGURE 41 - STEM Image 04

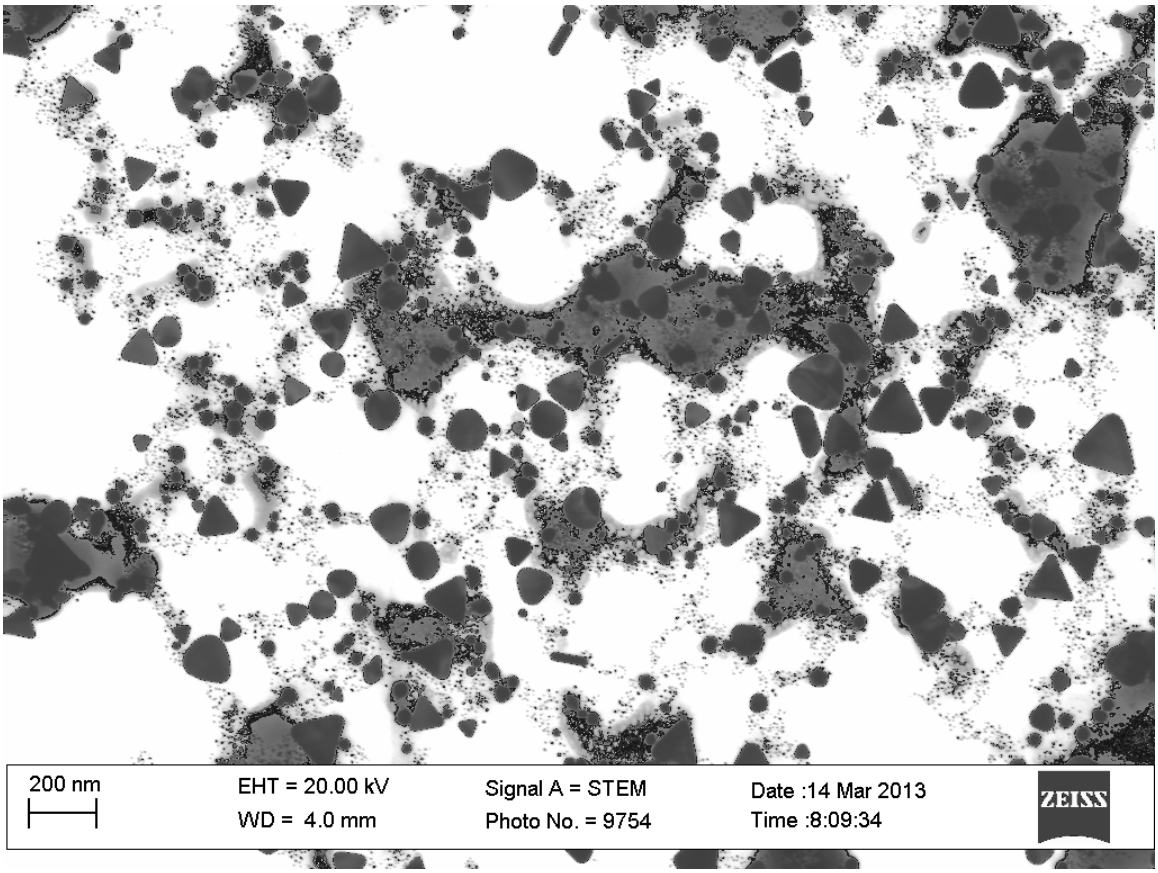

FIGURE 42 - STEM Image 05

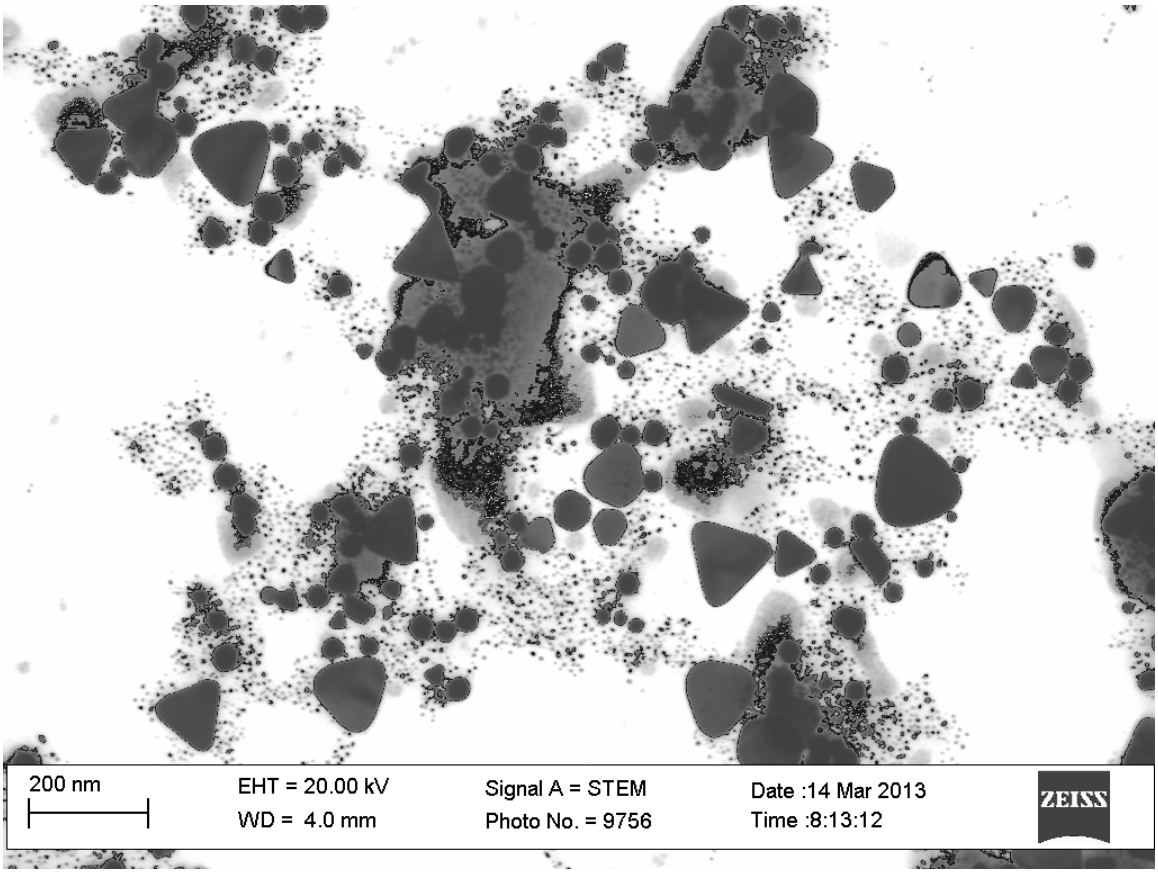

FIGURE 43 - STEM Image 06

REFERENCES

Atwater, H.A. and Polman, A. (2010). “Plasmonics for improved photovoltaic devices.” *Nature Materials* **9:** 205-213.

Averitt, R., Sarkar, D., and Halas, N. (1997). “Plasmon Resonance Shifts of Au-Coated Au2S Nanoshells: Insight into Multicomponent Nanoparticle Growth” *Physical Review Letters* **78:** 4217-4220.

Averitt, R.D., Westcott, S.L., and Halas, N.J. (1999). “Linear optical properties of gold nanoshells.” *Journal of the Optical Society of America* **16**: 1824–1832.

Azzazy, H., and Mansour, M. (2009). “In vitro diagnostic prospects of nanoparticles.” *Clinica Chimica Acta* **403**: 1–8.

Bode, A. and Dong, Z. (2009). “Cancer prevention research-then and now.” *Nature Review Cancer* **9**:508–516.

Cai, W., Gao, T., Hong, H., and Sun, J. (2008) “Applications of gold nanoparticles in cancer nanotechnology.” *Nanotechnology, Science and Applications* **1:** 17–32

Cao, Y.C., Jin, R., and Mirkin, C.A. (2002). “Nanoparticles with Raman Spectroscopic Fingerprints for DNA and RNA Detection” *Science* **297**: 1536-1540.

Chandran, S.P., Chaudhary M., Pasricha R., Ahmad, A. and Sastry, M. (2006) “Synthesis of Gold Nanotriangles and Silver Nanoparticles Using *Aloe* v*era* Plant Extract” *Biotechnology Progress* **22**: 577-583.

Diao, J. and Chen, H. (2006). “Near infrared surface plasmon resonance of gold tabular nanostructures in the HAuCl4–Na2S reaction.” *The Journal of Chemical Physics* **124**: 116103.

El-Sayed, I., Huang, X., and El-Sayed, M. (2005). “Surface Plasmon Resonance Scattering and Absorption of anti-EGFR Antibody Conjugated Gold Nanoparticles in Cancer Diagnostics: Applications in Oral Cancer.” *Nano Letters* **5:** 829-834**.**

Faraday, M. (1857). “The Bakerian Lecture: Experimental Relations of Gold (and Other Metals) to Light.” *Philosophical Transactions of the Royal Society* **147:** 145-181.

Gobin, A.M., Watkins, E., Quevedo, E., Colvin, V., and West, J. (2010). “Near-Infrared-Resonant Gold/Gold Sulfide Nanoparticles as a Photothermal Cancer Therapeutic Agent” *Small* **6**: 745-752.

Gosh, S.K. and Pal, T. (2007). "Interparticle Coupling Effect on the Surface Plasmon Resonance of Gold Nanoparticles: From Theory to Applications." *Chemical Reviews* **107**: 4797-4862.
He, J., Kunitake, T., and Nakao, A. (2003). " Facile In Situ Synthesis of Noble Metal Nanoparticles in Porous Cellulose Fibers." *Chem. Mater*. **15:** 4401-4406.

Hirsch, L., Stafford, R., Bankson, J., Sershen, S., Rivera, B., Price, R., Hazle, J., Halas, N., and West, J. (2003). "Nanoshell-mediated near-infrared thermal therapy of tumors under magnetic resonance guidance." *PNAS* **100**: 13549–13554.

Huang, D., Liao, F., Molesa, S., Redinger, D., and Subramanian, V. (2003). "Plastic-Compatible Low Resistance Printable Gold Nanoparticle Conductors for Flexible Electronics." *Journal of Electrochemical Society* **150**: G412-G417.

Huang, X., Jain, P., El-Sayed, I., and El-Sayed, M. (2008). "Plasmonic photothermal therapy (PPTT) using gold nanoparticles*." Lasers Med. Sci*.**23**: 217–228.

Ito, Y, Kennan, R.P., Watanabe, E., and Koizumi H. (2000). "Assessment of heating effects in skin during continuous wave near infrared spectroscopy." *J. Biomed Opt.* **5**:383-390.

Jain, S., Hirst, D., and O'Sullivan, J.M. (2012). "Gold nanoparticles as novel agents for cancer therapy." *The British Journal of Radiology* **85**: 101–113.

Klar, T., Perner, M., Grosse, S., von Plessen, G., Spirkl, W., and Feldmann, J. (1998). "Surface-Plasmon Resonances in Single Metallic Nanoparticles." *Physical Review Letters* **80**: 4249-4252.

Link, S. and El-Sayed, M.A. (1999a). "Spectral Properties and Relaxation Dynamics of Surface Plasmon Electronic Oscillations in Gold and Silver Nanodots and Nanorods." *J. Phys. Chem. B* **103**: 8410-8426.

Link, S. and El-Sayed, M.A. (1999b). "Size and Temperature Dependence of the Plasmon Absorption of Colloidal Gold Nanoparticles." *Journal of Physical Chemistry* **103:** 4212-4217.

Liu, X., Atwater, M., Wang, J., and Huo, Q. (2006). "Extinction coefficient of gold nanoparticles with different sizes and different capping ligands" *Colloids and Surfaces B: Biointerfaces* **58**: 3–7.

Loo, C., Lin, A., Hirsch, L., Lee, M., Barton, J., Halas, N., West, J., Drezek, R. (2004). "Nanoshell-Enabled Photonics-Based Imaging and Therapy of Cancer." *Technology in Cancer Research & Treatment* **3:** 33-40.

Mie, G. (1908). "Contributions to the optics of turbid media, particularly of colloidal metal solutions." *Ann. Phys*. **25**,: 377-445.

Morris, T., Copeland, H., and Szulczewski, G. (2002). “Synthesis and Characterization of Gold Sulfide Nanoparticles.” *Langmuir* **18**: 535-539.

Millstone, J., Hurst, S., Me´traux, G., Cutler, J., and Mirkin, C. (2009). “Colloidal Gold and Silver Triangular Nanoprisms.” *Small* **5:** 646-664.

Nikoobakht, B. and El-Sayed, M. A. (2003). “Preparation and Growth Mechanism of Gold Nanorods (NRs) Using Seed-Mediated Growth Method.” *Chem. Mater.* **15**: 1957-1962

Oldenburg, S.J., Averitt, R.D., Westcott, S.L., Halas, N.J. (1999). “Nanoengineering of optical resonances.” *Chemical Physics Letters* **288**: 243–247.

Patel, Dhruvinkumar. 2012. A Novel High Yield Process For Gold Sulfide Nanoparticle Synthesis Via Shifting Equilibrium of Self-Assembling Reaction. Master of Engineering thesis, University of Louisville.

Pinto, R. and Neves, M. (2012). Composites of Cellulose and Metal Nanoparticles. In *Nanocomposites - New Trends and Development* (pp. 73-96). InTech

Schwartzberg, A.M., Grant, C.D., van Buuren, T., and Zhang, J.Z. (2007). “Reduction of $HAuCl_4$ by Na_2S Revisited: The Case for Au Nanoparticle Aggregates and Against Au_2S/Au Core/Shell Particles.” *J. Phys. Chem. C* **111**: 8892-8901.

Thompson, D.(2007). “Using gold nanoparticles for catalysis” *NanoToday* **2**: 40-43.

Tréguer-Delapierre, M., Majimel, J., Mornet, S., Duguet, E., Ravaine, S. (2008). “Synthesis of non-spherical gold nanoparticles.” *Gold Bulletin* **41**: 195-207.

Weissleder, R. (2001). “ A clearer vision for in vivo imaging.” *Nature Biotechnology* **19**: 316-317.

Willets, K. and Van Duyne, R. (2007). “Localized Surface Plasmon Resonance Spectroscopy and Sensing.” *Annu. Rev. Phys. Chem*. **58**: 267–97.

Young, J., Figueroa, E., and Drezek, R. (2012). “Tunable Nanostructures as Photothermal Theranostic Agents.” *Annals of Biomedical Engineering* **40**: 438–459.

Young, K., Jones, M., Zhanga, J. Macfarlanea, J., Esquivel-Sirventa, R., Nape, R., Wuc, J., Schatza, G., Leef, B., and Mirkin, C. (2012). “Assembly of reconfigurable one-dimensional colloidal superlattices due to a synergy of fundamental nanoscale forces.” *PNAS* **109:** 2240-2245.

Yu, Y., Chang, S., Lee, C., and Wang, C. (1997). “Gold Nanorods: Electrochemical Synthesis and Optical Properties.” *J. Phys. Chem. B* **101:** 6661-6664

Zharov, V.P., Mercer, K.E., Galitovskaya, E.N., Smeltzer, M.S. (2006). "Photothermal Nanotherapeutics and Nanodiagnostics for Selective Killing of Bacteria Targeted with Gold Nanoparticles." *Biophysical Journal* **90**: 619-627.

Zhang, G., Jasinski, J., Howell, J., Patel, D., Stephens, D., and Gobin, A.M. (2012). Tunability and stability of gold nanoparticles obtained from chloroauric acid and sodium thiosulfate reaction." *Nanoscale Res Lett.* **7**: 337.

Zhou, H.S., Honma, I., and Komiyama, H. (1994). "Controlled synthesis and quantum-size effect in gold-coated nanoparticles." *Physical Review B* **50**: 12052-12056.